BMPS REGULATE THE OFT DEVELOPMENT VIA MIRNAS

A Dissertation

by

YAN BAI

Submitted to the Office of Graduate and Professional Studies
Texas A&M University
in partial fulfillment of the requirements for the degree of

DOCTOR OF PHILOSOPHY

Chair of Committee,	Mingyao Liu
Co-Chair of Committee,	James F. Martin
Committee Members,	Richard Behringer
	Dekai Zhang
Head of Department,	Fen Wang

August 2014

Major Subject: Medical Sciences

ABSTRACT

Congenital heart diseases (CHD) are the leading cause of infant mortality and morbidity. Defects of the outflow tract (OFT) make up a large percentage of human CHD. In my study, I focused on the role of Bone morphogenetic protein (BMP) on heart development. I investigated Bmp signaling in OFT development using conditional knocking out Bmps, including *Bmp2*, *-4* and *-7*. Deletion of *Bmp4/7* in second heart field (SHF) results in persistent truncus arteriosus (PTA), which is caused by endothelial to mesenchyme transition (EMT) defect. I found that *Vegfa* (vascular endothelial growth factor a) is a downstream target of *Bmp* and *miR-17-92*. Repression of *Vegfa* in OFT is important for the proper onset of EMT at E10.5. Further exploration on *Bmp2/4/7* mutation indicates that loss of Bmp signal disrupt the smooth muscle differentiation and maintenance. Similar with observations on Marfan syndrome mouse model, *Bmp2/4/7* triple CKO embryos exhibited significant upregulation of Tgf-β signal activity. Alternation of SMC feature is likely due to the persistence of *Isl-1* expression. Haploinsufficiency of *Bmp4* triggered early onset of aorta aneurysm in *Fbn-1*$^{C1039G/+}$ mice. These data indicate that Bmps not only play an important role in embryonic cardiogenesis, but also are critical for the cell fate differentiation and maintenance in adulthood.

ACKNOWLEDGEMENTS

I would like to express my deepest appreciation to all those who provided me the possibility to complete my project. A special gratitude and thanks to my mentor, Professor Dr. James Martin for the stimulating suggestions, useful comments and encouragement through all these years.

I would like to thank all my committee members, Professor Dr. Behringer, Professor Dr. Liu and Professor Dr. Zhang, for their brilliant guidance and support throughout the course of this research.

I would like to acknowledge with much appreciation the crucial role of the staff of Texas A&M Health Science Center and Baylor College of Medicine, Cynthia Lewis, Smantha Del Castillo, Mary Cole, Janis Bender, Deborah Colbert, Lynda Attaway and Ross Adkins. A special thanks goes to current and previous lab members for their help and friendship, Jun Wang, Yuka Morikawa, Yang Xiao, Margarita Bonilla-Claudio, Ye Tao, Stephanie Greene, Min Zhang, Ge Tao, Todd Heallen, John Leach, Tanner Monroe, Matthew Hill, Yocheved Schindler and Lele Li. I would like to thank lab technicians for their technical help, especially Elzbieta Klysik, Meifang Lu, Thuy Tien Tran, Mahdis Rahmani and Paul Swinton. Part of this work was supported by my pre-doctoral fellowship from the American Heart Association (#12PRE11720003).

Finally, thanks to my family for their love, encouragement and support.

Part of this thesis is reproduced/adapted with permission from “Bmp signaling represses vegfa to promote outflow tract cushion development“ by Yan Bai, Jun Wang,

Yuka Morikawa, Margarita Bonilla-Claudio, Elzbieta Klysik and James Martin, Development 140, 3395-3402 (2013), doi: 10.1242/dev.097360.

NOMENCLATURE

AAA	Abdominal Aorta Aneurysm
AP	Aorta-Pulmonary
AVC	Atrioventricular Canal
BMP	Bone Morphogenetic Protein
CDK	Cyclin-Dependent Kinase
CHD	Congenital Heart Disease
ChIP	Chromatin Immunoprecipitation
CKO	Conditional Knock Out
CNC	Cardiac Neural Crest
ECM	Extracellular Matrix
EMT	Endothelial to Mesenchyme Transition
FBN	Fibrillin
FDA	Food and Drug Administration
JNK	c-Jun N-terminal Kinase
LAP	Latency Associated Peptide
LLC	Large Latent Complex
LTBP	Latent Tgf-β Binding Protein
MFS	Marfan Syndrome
miR	microRNA
OFT	Outflow Tract
PFA	Paraformaldehyde

PHF	Primary Heart Field
PPE	Pancreatic Elastase
PTA	Persistent Truncus Arteriosus
SBE	Smad Binding Element
SHF	Second Heart Field
SLC	Small Latent Complex
SMAD	Small Mothers Against Decapentaplegic
SMC	Smooth Muscle Cell
TAA	Thoracic Aorta Aneurysm
TGF-β	Transforming Growth Factor β
THF	Tertiary Heart Field
UTR	Untranslated Region
VEGFA	Vascular Endothelial Growth Factor A
VSD	Ventricular Septum Defect
VV	Vasa Vasorum

TABLE OF CONTENTS

Page

ABSRACT ii

ACKNOWLEDGEMENTS iii

NOMENCLATURE v

TABLE OF CONTENTS vii

LIST OF FIGURES viii

LIST OF TABLES ix

CHAPTER I INTRODUCTION AND LITERATURE REVIEW 1

CHAPTER II BMP SIGNALING REPRESSES VEGFA TO PROMOTE OUTFLOW TRACT CUSHION DEVELOPMENT 8

- Background and significance 8
- Materials and methods 11
- Results 15
- Discussion 30
- Summary 33

CHAPTER III BMP SIGNALING DISRUPTION IN SHF IMPAIRS AORTA DEVELOPMENT AND EARLIER ONSET OF AORTA ANEURYSM 35

- Background and significance 35
- Materials and methods 39
- Results 42
- Discussion 56
- Summary 61

CHAPTER IV CONCLUSION 63

REFERENCES 66

APPENDIX 79

LIST OF FIGURES

FIGURE Page

1 Persistent truncus arteriosus 2

2 Heart fields in mouse embryo cardiogenesis 3

3 Epithelial mesenchymal transformation 4

4 Bone morphogenetic protein signal pathway 6

5 Inactivation of *Bmp2*, *-4* and *-7* in SHF 16

6 Transcription modulation of *Vegfa* by Smad 20

7 *miR-17/20a* are downstream effectors of Bmp signaling 24

8 *Ex vivo* collagen gel assay of the OFT 26

9 Rescue of *Bmp4/7* deficiency by conditionally overexpressiong of *miR-17-92* 27

10 Molecular mechanism on Bmp regulation of OFT development 34

11 Study strategy for Bmp function assay on aorta 42

12 Haploinsufficiency of Bmp exacerbates aorta aneurysm in *Fbn-1*$^{C1039G/+}$ mice 44

13 *Bmp2/4/7* ablation results in OFT abnormality 46

14 Bmp positively regulate *Fbn-1* 48

15 Activation of *Tgf-β* signal in the absence of *Bmp2/4/7* 50

16 *Bmp2/4/7* ablation results in disruption of smooth muscle cell fate 52

17 *miR-17-92* overexpression partially restores the phenotype 53

18 Working model of Bmp regulation in aorta aneurysm 55

19 Working model of Bmp regulation in OFT and aorta maintenance 65

LIST OF TABLES

TABLE Page

1 Defects observed in *Bmp2/4/7* conditional knockout embryos at E14.5..... 18

2 OFT phenotype in *Bmp4/7* mutant..... 29

CHAPTER I

INTRODUCTION AND LITERATURE REVIEW

Congenital heart diseases (CHD) occur in nearly 1% of all live births and are the leading cause of infant mortality and morbidity in the western world. Anomaly of OFT occurs at a frequency of approximately 1/3 of congenital heart diseases. Disturbance of the morphogenetic patterning of the anterior pole of the heart is a cause for a variety of OFT defects, while this patterning is essential for separation of systemic and pulmonary circulations. Persistent truncus arteriosus (PTA) is a most severe phenotype of OFT defect, with unfavorable prognosis since complete surgical repair is not always possible (Williams et al., 1999). Ventricular septal defect (VSD) is always associated with PTA defect (Fig. 1), open heart surgery is needed if the opening is large to prevent serious problem. Though robust studies of possible genetics causes would provide insight into the pathogenesis of CHD, but, the etiology of most CHD, including OFT defects remains unknown because of the multifactorial nature of the diseases (Bruneau, 2008; Olson, 2006; Yamagishi et al., 2009; Zhao and Srivastava, 2007).

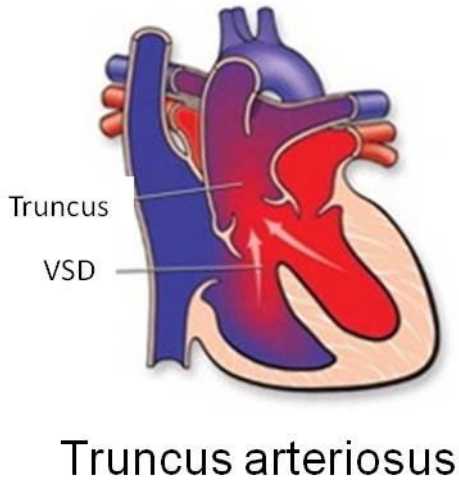

Figure 1. Persistent truncus arteriosus. Persistent truncus arteriosus (PTA) is a common congenital heart defect of OFT. As showing in this cartoon, patient has one large artery instead of separated aorta and pulmonary artery. VSD is associated with PTA defect. Diagram from American heart association website. http://www.heart.org/HEARTORG/Conditions/CongenitalHeartDefects/AboutCongenitalHeartDefects/Truncus-Arteriosus_UCM_307040_Article.jsp

As the first formed and functional organ in vertebrates, the heart has a pivotal role in distribution of nutrients and oxygen to support normal embryogenesis and development. At the earliest stage of cardiogenesis (E7.5), cardiac crescent, there are two groups of cardiac precursors exist: the primary heart field (PHF) and the second heart field (SHF) (Fig. 2). The PHF will eventually contribute to the left ventricle part of atriums and right ventricle. The SHF will give rise to the OFT, right ventricle and portion of atrium (Brand, 2003; Harvey, 2002; Koshiba-Takeuchi et al., 2009). Cardiac Neural Crest (CNC) is also involved in parts of hearts. Recent study discovered the tertiary heart field (THF) in chicken embryo, which is responsible for the cardiac

pacemaker cells, a discrete region of mesoderm outside of PHF and SHF(Bressan et al., 2013). The linear heart tube starts beating at E8.0, and after looping process, the heart

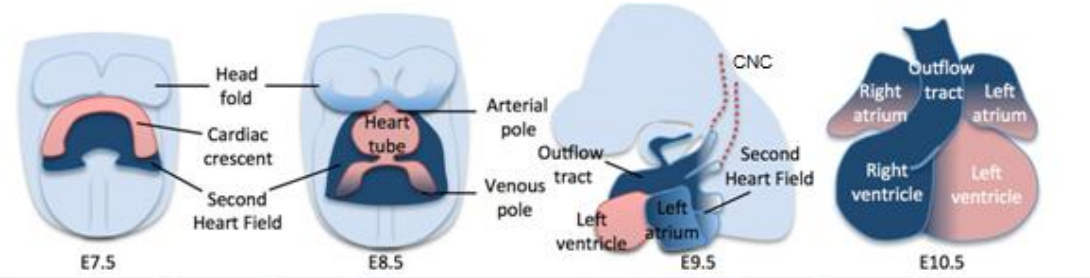

Figure 2. Heart fields in mouse embryo cardiogenesis. First heart field (FHF) is marked as pink and second heart field (SHF) is in blue. FHF will eventually give rise to left ventricle, part of atrium, while SHF will contribute to right ventricle, outflow tract and portial of atrium. Cardiac neural crest (CNC) is also believed to be involved in the distal part of OFT development. Modified from http://www.ibdm.univ-mrs.fr/equipe/genetic-control-of-heart-development/

finally form four chambers around E10.0. The heart tube is composed of a contractile myocardium, an inner lining endothelium and cardiac jelly in between. The OFT first originates as a cardiomyocyte-lined vascular channel through which blood exits the primitive ventricle and fills the aortic sac (Vincentz et al., 2008). At E10.5, the OFT cushion is invaded by mesenchymal cells, which delaminate from the endocardium and undergo an epithelial-mesenchymal transformation (EMT) characterized by the expression of α-smooth muscle actin. As development proceeds, continued expansion of

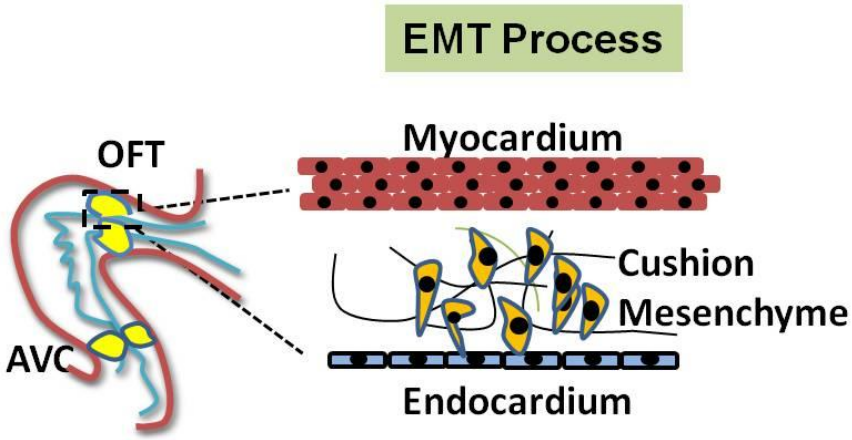

Figure 3. Epithelial-mesenchymal transformation. During the EMT process, signals from myocardium tell the endocardium cells to delaminate, migrate and invade into the cardiac jelly, to form cushion mesenchyme. Those cushion mesenchyme will eventually contribute to valve formation, septation of the OFT, and the interventricular septum. EMT occurs at OFT around E10.5, and AVC around E9.5.

these mesenchymal cells is critical for both aorta-pulmonary (AP) septation and valve formation (Fig. 3). At E14.5, the mouse heart develops into four chambers and the OFT is separated into aorta and pulmonary artery. Further remodeling of migrating mesenchymal cells will transforms cushions into fibrous leaflets. Atrioventricular (mitral and tricuspid, left and right respectively) and semilunar (aorta and pulmonary) valves have different morphology and individual morphogenesis. Semilunar valves can prevent backflow of the blood from the aorta and pulmonary trunks into the ventricles (Dalot et al., 2003). The cardiac neural crest also contributes to the AP septum and the OFT cushions, it is destined to distal OFT according to recent reports (Liu et al., 2004). EMT process is also occurred at AV canal at around E9.5, which is indispensable for the

development of AV cushion formation and subsequently heart septum and associated valves to transit heart tube to chamber organ.

Bone morphogenetic proteins (BMPs) are growth factors and cytokines. Bmps belong to TGF-β (Transforming growth factor β) super family. These proteins are active as homo- or heterodimer, linked by a single disulfide bond. Based on the sequence similarities, *TGF-β* family can be subdivided into TGF-β, Activin, Nodal and Bmp. Despite the diversity of TGF-β members in the whole animal kingdom, all members of the super family share similar structure and scheme of synthesis. Firstly, TGF-β is synthesized as a large precursor protein with N-terminal region called the mature TGF-β and the C-terminal pro-region referred to latency-associated peptide (LAP). A dimer of the C-terminal peptide is either released or associated with the mature TGF-β to form a latent complex, which binds to latent TGF-β binding protein (LTBPs). The presence of LAP facilitates transit of TGF-β from the cell to matrix and keeps the TGF-β ligand biologically inactive state (Khalil, 1999). Secondly, this complex will be catalyzed by proteinases such as plasmin, releasing of active TGF-β from LAP and resulting in the activation of TGF-β ligands. Activated TGF-β ligands bind to constitutively phosphorylated type II receptors through extracellular domain, resulting recruitment and transphosphorylation of type I receptors. TGF-β signal pathway effector, R-Smad (Smad1/5/8 for BMP signal pathway and Smad2/3 for TGF-β), will be recruited and phosphorylated to dimerism with Co-smad (smad4). This complex will shuttle from cytoplasm to nucleus to execute their roles in transcriptional regulation. In the nucleus, Smads modulate transcription of target genes by direct binding to DNA, interaction with

other DNA-binding proteins, or recruiting co-activators/repressors (Kawabata et al., 1998) (Fig. 4). Phospho-Smad has been shown to regulate transcription in both positive and negative way (Kawabata et al., 1998). A c-terminal phosphatase can de-phosphorylate R-smad to terminate the signaling cascade. However, it is reported that there is constant cytoplasm-nucleus shuttling of R-Smad and Co-Smad which is independent on phosphorylation signal. Besides, CDK8/9 is reported to phosphorylate

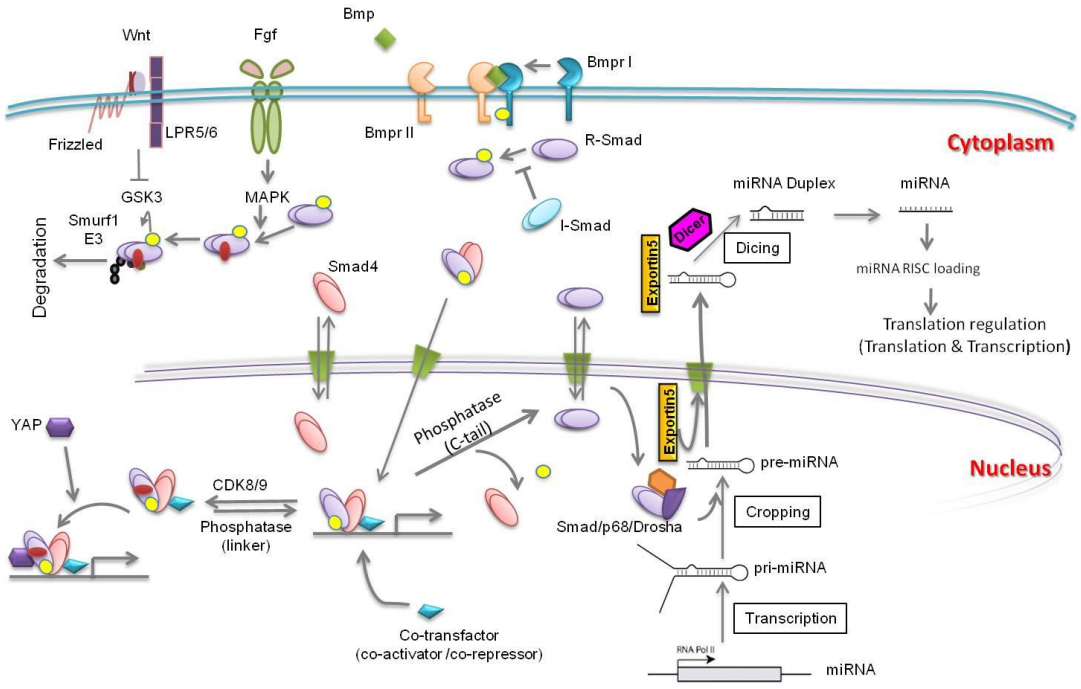

Figure 4. Bone morphogenetic protein signal pathway. Diagram shows BMP signal pathway and its involvement of microRNA biogenesis. Upon binding to Bmp receptor II, Bmp ligands phosphorylate Bmp receptor I and activate R-smad. R-smad/Smad4 complex regulate its target genes by co-transfactors. Smad/p68/Drosha is reported to facilitate cropping of pri-miRNA to pre-miRNA.

the linker region of Smad protein, which recruits YAP and subsequent transcription regulation (Alarcon et al., 2009) (Fig. 4).

It is reported that Smads alone can directly binding to certain DNA motifs, but with low affinity and selectivity (Itoh et al., 2000; Karaulanov et al., 2004; Shi and Massagué, 2003; Zwijsen et al., 2003). Therefore, to ensure its regulation of its target gene, Smads have to associate with various transcription factors to form R-Smad/Co-Smad/Co-TF complex (Zwijsen et al., 2003). R-Smads and Smad4 can recognize Smad binding element (SBE) motif GTCTG (Shi, 1998). GCAT was described as a Smad1 binding element in the promoter of *Xenopus Vent2* (Henningfeld et al., 2000). GCCG core consensus is believed to be Smad binding motif in several vertebrate BMP-responsive promoters, such as *Smad6* (Ishida et al., 2000) and *Id1* (Korchynskyi and ten Dijke, 2002). Karaulanov et al. identified TGGCGCC, a BMP-responsive element, is highly prognostic for BMP-responsive enhancers (Karaulanov et al., 2004).

CHAPTER II

BMP SIGNALING REPRESSES VEGFA TO PROMOTE OUTFLOW TRACT CUSHION DEVELOPMENT[*]

Background and Significance

BMPs are named by their ability to induce bone and cartilage formation. There are about over 20 different BMPs have been identified in various species (Hogan, 1996). Excitingly but not surprisingly, recombinant BMP2 and BMP7 are approved by the Food and Drug Administration (FDA) in the clinical use of spine fusion, fracture healing and oral surgery (Nakashima and Reddi, 2003; Reddi, 1998). Besides bone formation, BMPs are also involved in morphogenesis of different organs and pathological processes. Studies show that BMPs are required for the OFT morphogenesis and BMP knock-out mice have a cushion defect phenotype during cardiogenesis (Liu et al., 2004). Bmp2/4 bind to BMPR-IA and BMPR-IB, Bmp6/7 strongly bind to ALK-2, but weakly to BMPR-IB (Kawabata et al., 1998; Miyazono et al., 2010). Diversity of receptors, different binding affinity and preference make BMP signaling complex. During development, BMPs and their receptors are expressed at many sites in which epithelial mesenchymal interactions occur, suggesting that BMPs play critical roles in early embryogenesis and organogenesis (Jones et al., 1991; Zhang and Bradley, 1996).

[*] This work has been published in Development. Bai, Y., Wang, J., Morikawa, Y., Bonilla-Claudio, M., Klysik, E., and Martin, J.F. (2013). Bmp signaling represses Vegfa to promote outflow tract cushion development. Development *140*, 3395-3402.

Bmp4 is expressed in splanchnic and branchial arch mesoderm, which contribute to the OFT and right ventricle development. *Nkx2.5-Cre* conditional ablation of *Bmp4* resulted in defects of the OFT septation, myocardium differentiation and assembly of vascular smooth muscle to vessels (Liu et al., 2004). *Bmp2* is involved in AV cushion development and essential for the invasive EMT (Luna-Zurita et al., 2010; Ma et al., 2005). *Bmp7* is less characterized and its single knock-out has no phenotype due to BMP functional redundancy. The *Bmp4* mutant embryos show variability in phenotype and incomplete penetrance, possibly due to functional redundancy of Bmp ligands. Although ablation of Bmp7 has no obvious phenotypic consequences in the hearts (Solloway and Robertson, 1999), loss of Bmp4 causes up-regulation of Bmp7 in OFT myocardium and compound mutants have a more severe phenotype (Liu et al., 2004). Overlapping expression of the Bmp ligands in the OFT and their function redundancy makes functional analysis of Bmp ligands in OFT development challenging.

Wnt1-Cre derived deficiency of type I Bmp receptors, *Alk2* and *Alk3*, results in severe OFT defects, with the *Cre* activity in CNC (Kaartinen et al., 2004; Stottmann et al., 2004). Ablation of *Bmp type 1 receptor a* (*Bmpr1a*) under *Tie2-Cre* in endocardium caused failure of cushion formation, suggesting that Bmp signal is pivotal for cushion forming endocardium to undergo EMT process (Stottmann et al., 2004). Analysis of a hypomorphic allele of the ubiquitously expressed *Bmp type II receptor (Bmpr2)*, lacking half of the ligand-binding domain, revealed defective proximal OFT septation in mouse embryos (D d ot et al., 2003).

Recent studies have shown that Bmp signaling also regulates downstream genes through miRNA maturation. In vascular smooth muscle, TGF-β- and BMP-specific SMAD is recruited to p68 (DDX5) RNA helicase containing complex. The SMAD/p68 complex interacts with Drosha in the nucleus to regulate miRNA biogenesis of a subset of miRNAs. This complex get access to pri-miR-21 to regulate miR-21 biogenesis (Davis et al., 2008). During cardiac development, *Bmp2/4* regulate the OFT myocardial differentiation by promoting transcription of the *miR-17-92* cluster (Wang et al., 2010). The *miR-17-92* cluster encodes six miRNAs, miR-17, miR-18a, miR-19a, miR-20a, miR19b-1 and miR-92-1. They are known as oncogenes and play roles in the development of heart, lungs and immune system (Koralov et al., 2008; Ventura et al., 2008; Vincentz et al., 2008; Xiao et al., 2008).

In this study, we discovered that loss of *Bmp4/7* in SHF resulted in PTA with up-regulation of *Vegfa*, repression of which is required in the atrioventricular canal (AVC) to promote EMT (Chang et al., 2004). Our *in vitro* studies showed that *Vegfa* was repressed by both Smad and *miR-17/20a*. Moreover, *in vivo* and *ex vivo* studies showed overexpression of *miR-17-92* or repression of *Vegfa* can partially suppress the Bmp loss of function phenotype. Our study reveals that in the OFT EMT and CNC influx is regulated by Bmp via a combination of Smad- and miR-dependent *Vegfa* repression.

Materials and Methods

Mouse lines

The *Bmp4* flox, *miR-17-92* null and *miR-17-92*^{OE} alleles and *Mef2c-Cre* lines have been previously described (Liu et al., 2004; Ventura et al., 2008; Verzi et al., 2005; Xiao et al., 2008). To generate the Bmp7flox allele, a targeting vector was constructed that introduced one loxP site into upstream of the *Bmp7* fourth exon followed by a frt flanked PGKneo cassette while another loxP site was introduced into downstream of the *Bmp7* fourth exon (See A-1). *miR- 17-92* LacZ transgenic mice is previously described (Wang et al., 2013).

β-galactosidase staining, histology, and immunostaining

Embryos were fixed overnight in 4% PFA (paraformaldehyde) or buffered formalin, dehydrated through graded ethanol, and paraffin embedded. Sections were cut at 7 μm and used for H&E staining or immunostaining. LacZ expression on whole embryos was performed as previously described (Lu et al., 1999). For Twist1 immunodetection, sections were deparaffinized and hydrated. And 10 mM citrate buffer was used for antigens retrieval. Monoclonal anti-Twist1 (1:200 dilution) (abcam, ab50887) was used as primary antibody. HRP-conjugated anti-mouse secondary antibody (Bio-Rad Co., Hercules, CA) was used and visualized using TSA^{TM} plus Fluorescence Systems from PerkinElmer (Boston, MA). Nuclei were stained with 4',6-Diamidino-2-Phenylindole, Dihydrochloride (Dapi) (invitrogen).

Quantitative real time RT-PCR

Total RNA from OFT (E10.5 embryos) was isolated using the RNeasy Micro Kit (QIAGEN). SuperScript II Reverse Transcriptase (Invitrogen) was used for RT-PCR with 20 ng-100 ng of mRNA, and SYBR Green JumpStart Taq ReadyMix (Sigma) was used for real time thermal cycling in triplicate reactions on StepOnePlus Real-Time PCR system (ABI); *Gapdh* was used as internal control. *Vegfa* was detected by TaqMan Probe (IDT, Mm.PT.47.7135538.g) and 18s rRNA (IDT) as internal control. For miRNAs, TaqMan microRNA assay kits (Applied Biosystems) were used according to manufacturer's guidelines. *Sno-202* was used as internal control. All error bars represent SEM. For all qRT-PCR experiments, at least 4 mutants and 4 controls embryos were analyzed. Primer sequences are available in A-2.

Sequence analysis and miRNA target predictions

For sequence analysis and alignment, NCBI (http://www.ncbi.nlm.nih.gov/), Ensemble (http://uswest.ensemble.org/Mus_musculus/Info/Index), rVista 2.0 (http://rvista.dcode.org/), and TFSEARCH (http://mbs.cbrc.jp/research/db/TFSEARCH.html) were used. For miRNA targets predictions, miRanda (http://www.microrna.org), TargetScan (http://www.targetscan.org) and miRDB (http://mirdb.org/miRDB/) were used.

Generation of constructs

To generate *Vegfa* promoter luciferase reporter plasmid, 1563 bp of *Vegfa* promoter was amplified using a high-fidelity PCR system (Roche) and subcloned into pGL3-Basic vector (Promega). To generate *Vegfa* 3'UTR luciferase reporter plasmid,

1881 bp *Vegfa* 3'UTR genomic sequence was amplified using a high-fidelity PCR system (Roche) from cDNA clone (#6816435, Open Biosystems) and subcloned into the pMIR-REPORT^{TM} Luciferase miRNA Expression Reporter Vector (Ambion). Site-directed mutagenesis of the seed sites in *Vegfa* 3'UTR and *Vegfa* promoter were performed with QuickChange II Site-Directed Mutagenesis Kit (Stratagene). All primers are available in A-2.

Luciferase activity assay

P19 cells were transfected with promoter and 3'UTR reporter plasmids described above using Lipofectamine 2000 (Invitrogen). Luciferase activity assays were performed using the Dual-Luciferase® Reporter assay system (Promega). The renilla luciferase encoding plasmid pRL-TK is used as normalization control. Ca-Alk3 (Wang et al., 2010) was used to activate Smad-pathway. miRNA mimics were purchased from Thermo Scientific.

***Ex vivo* OFT explant culture**

A solution (1.5 mg/ml) of rat-tail collagen type I (BD Biosciences) was dispensed into 24 well microculture dishes and allowed to solidify inside a 37 ℃, 5% CO_2 incubator. Collagen gels were washed several times with DMEM containing 10% FBS, 0.1% insulin-transferrin-seleniun (ITS, GIBCO; Invitrogen), and streptomycin (Invitrogen). OFTs were harvested in sterile Tyrode's Salt Solution (Sigma-Aldrich) from E10.5 embryos. OFT were carefully dissected, and endocardium was exposed to the collagen gel, with myocardium overlaying. 4 hours after attachment, medium (100 μl/well) was added and explants cultured for up to 3 days. Explants were fixed and

stained with α-SMA-Cyan3 (1:100; Sigma-Aldrich) to detected mesenchymal cells and phalloidin-FITC (1:100; Sigma-Aldrich) to reveal the actin cytoskeleton as described (Luna-Zurita et al., 2010). TO-PRO®-3 Iodide (TOP3) (invitrogen) was used for nuclei staining. For explants treatments, the medium was supplemented with sFlt (10 ng/ml; R&D system 471-F1). Medium was replaced every 24 hours.

***In vivo* chromatin immunoprecipitation**

About 80 OFT of E10.5 wild type embryos were dissected and subject to the chromatin immunoprecipitation (ChIP) analysis, soluble chromatin was prepared after formaldehyde crosslinking and sonication. Smad1/5/8 antibody (sc-6031 X, Santa Cruz) was used to immmunoprecipitate protein-bound DNA fragments. And normal rabbit immunoglobulin G was used as control. The PCR product for SBE1 fragment was 280bp, 402bp for SBE2 fragment, and 204bp for SBE3 fragment. Primers designed for irrelevant chromatin sequence to Smad were used as a negative control. SYBR is used for ChIP-qPCR and result is analyzed by percent input method described before. Primer sequences are available in A-2.

Results

Bmp2, -4, and -7 regulate EMT and have redundant functions

Bmp2, -4, and -7 show overlapping expression pattern and functional redundancy (Bonilla-Claudio et al., 2012; Dudley and Robertson, 1997; Furuta et al., 1997; Wang et al., 2010). We compared the expression patterns of *Bmp2*, *-4* , *-7* using *lacZ* knock-in mouse lines for *Bmp2* and *Bmp4* and *in situ* hybridization of *Bmp7*. *Bmp2* and *Bmp4* were expressed in the OFT at E9.5, while *Bmp7* was broadly expressed in entire heart tube (A-3, A-B,G-H,M-N). *Bmp4* expression was found in inflow tract at E9.5 but was limited to OFT at E10.5. Analysis of the sections revealed that *Bmp2, -4,* and *-7* were exclusively co-expressed in OFT myocardium (A-3, C,E,I,L,O,R). At E10.5, expression of *Bmp2* in the OFT was decreased (A-3, G,J), while *Bmp4* and *Bmp7* expression were maintained at similar levels (A-3, A,D and M,P).

To determine redundant functions of Bmp molecules, we deleted *Bmp2, -4* and *-7* in different combinations in the OFT using *Mef2c-Cre* (Fig. 5A-H). Proximal OFT mesenchymal cells of *Bmp2/4*, *Bmp4/7* and *Bmp2/7* dCKO were absent (Fig. 5C-F). *Bmp4* and *Bmp7* deletion resulted in OFT cushion defect in CNC-derived distal OFT, as well as, proximal OFT (Fig. 5D). The distal OFT defects were not observed by deleting *Bmp2* in *Bmp4* homozygous or heterozygous background, suggesting that *Bmp2* had restricted OFT function (Fig. 5C,F).

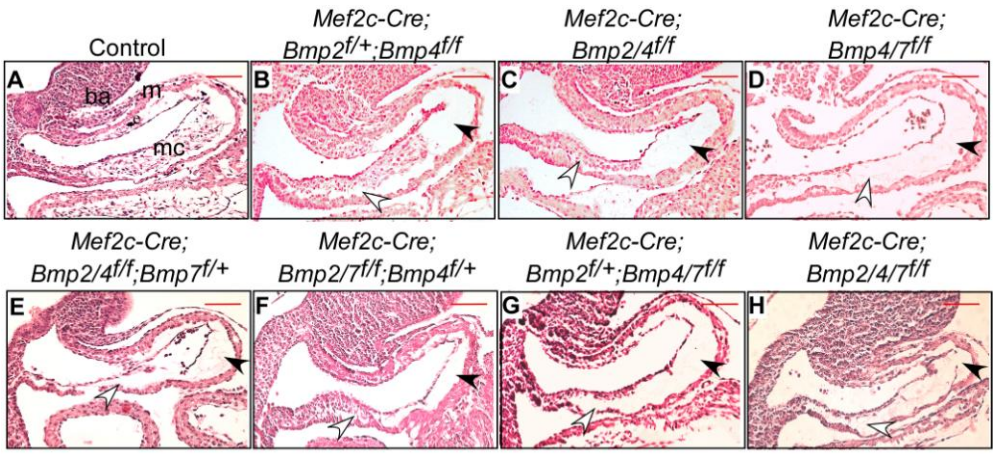

Figure. 5 Inactivation of *Bmp2, -4, and -7* in SHF. A-H: Sagittal sections of E10.5 embryos with different combination of *Bmp*s deletion. *Bmp*s were knocked out conditionally in SHF using *Mef2c-Cre*. Black arrowheads show proximal OFT and white arrowheads show distal OFT. Scale bar=100 μm. n=6, 5, 5, 6, 3, 2, 5, 5, corresponding to A-H. I-L: Whole mount hearts and sections of control and *Bmp4/7* dCKO at E14.5. Arrow in top panel represents PTA. ba: branchial arch; m: myocardium; mc: mesenchymal cushion; e: epithelium; ao: aorta; pa: pulmonary artery; la: left atrium; ra: right atrium; lv: left ventricle; rv: right ventricle; av: aorta valve; sv: semilunar valve; pta: persistent truncus arteriosus; ivs: interventricular septum; scale bar=100 μm (white), scale bar=500 μm (red). M-N: Immunostaining of Twist1 in control and *Bmp4/7* dCKO embryos at E10.5. Arrow points twist1 positive cells, scale bar=50 μm. O: Expression of EMT related genes were examined in the OFT of control and *Bmp4/7* dCKO embryos at E10.5. RT-PCR analysis was performed using SYBR for *Id1/2*, *snai1* and *slug* and Taqman for *Vegfa* (Control *n*=5, mutant *n*=4). *p*-value was analyzed by t-test (two-tailed). Error bars represent SEM. *<0.004, **=0.03, ***=0.04.

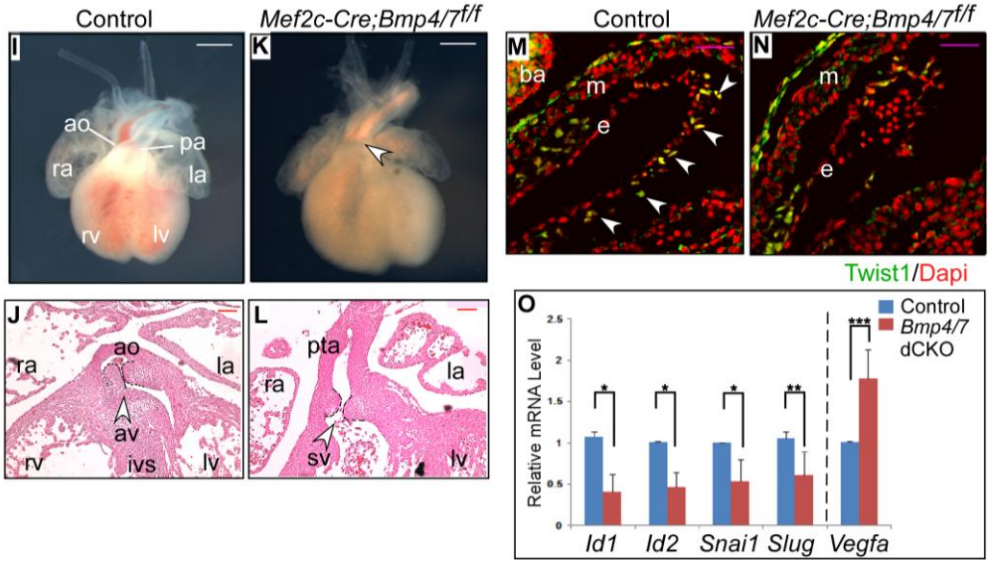

Figure 5 Continued.

Consistent with the defective CNC influx and proximal EMT observed at E10.5, *Bmp4/7* double mutants had severe OFT defects at E14.5 with failure of OFT separation resulting in PTA (Table 1, Fig. 5I-L). One *Bmp4/7* dCKO had double outlet right ventricle (DORV), with both aortic and pulmonary arteries draining the right ventricle (Table 1). In addition to defective great vessel separation, histological sections showed the hypoplastic semilunar valves and interventricular septal defect (VSD, data not shown) in *Bmp4/7* dCKO (Fig. 5J,L). Taken together, our findings revealed that *Bmp4* and *Bmp7* had redundant functions in OFT development. To further explore Bmp-signaling in the OFT, we focused on *Bmp4/7* dCKO mouse model.

Table 1 Defects observed in *Bmp2/4/7* conditional knockout embryos at E14.5

	OFT defects	
Genotype	PTA	DORV
Mef2c-Cre;Bmp4/7$^{f/f}$	6/7	1/7
Mef2c-Cre;BMP2$^{f/+}$BMP4/7$^{f/f}$	5/5	n/a
Mef2c-Cre;Bmp2/4/7$^{f/f}$	6/6	n/a

DORV: double outlet right ventricle, PTA: persistent truncus arteriosus

To investigate EMT process in *Bmp4/7* dCKO, we performed pHH3 analysis for cell proliferation and did not see obvious difference between control and *Bmp4/7* dCKO in the myocardium (data not shown). Immunostaining showed fewer Twist1 expressing mesenchymal cells in the OFT of *Bmp4/7* dCKO than the control (Fig. 5M-N), indicating that fewer cells progressed through EMT in the *Bmp4/7* mutant. To determine the mechanism of EMT regulation by Bmp, expression of the genes involved in Bmp pathway and EMT were examined by qRT-PCR. The Bmp-regulated EMT genes, *Snai1*, *Slug*, *Id1* and *Id2* were significantly decreased in *Bmp4/7* dCKO OFT while *Vegfa* was up-regulated by 1.8-fold (Fig. 5O).

Smad directly represses *Vegfa* transcription

The major downstream Bmp-signaling effectors are Smad proteins. To determine if *Vegfa* is a direct downstream target of Bmp, we searched for conserved Smad binding sites in *Vegfa* 5' upstream sequences by bioinformatics analysis. Analysis of *Vegfa* 5' upstream sequence predicted several conserved functional elements for Bmp response (McCulley et al., 2008) which are Smad binding elements (SBE) and Smad1 binding motif (s1). SBE motif is a canonical Smad binding sequence (Shi, 1998) and is found in the promoter of many TGF-β and Bmp responsive genes while the s1 motif is another sequence found in the promoter of Xenopus vent2. These motifs are usually flanked with BRE-like (Bmp Responsive Element) and/or GC-rich Boxes (Fig. 6A) which is common in regulatory elements of Bmp responsive genes. To test whether Smad directly binds *Vegfa* 5'upstream sequences, we performed *in vivo* chromatin immunoprecipitation (ChIP)-PCR analysis on wild-type E10.5 embryonic OFT. We detected enrichment in the anti-Smad1/5/8 ChIP-PCR for all three putative SBEs (Fig. 6B, C). ChIP-qPCR data further supported that those putative SBEs in *Vegfa* chromatin were bound by Smad (Fig. 6C). The results indicate that Smad1/5/8 can directly bind *Vegfa* chromatin in the OFT.

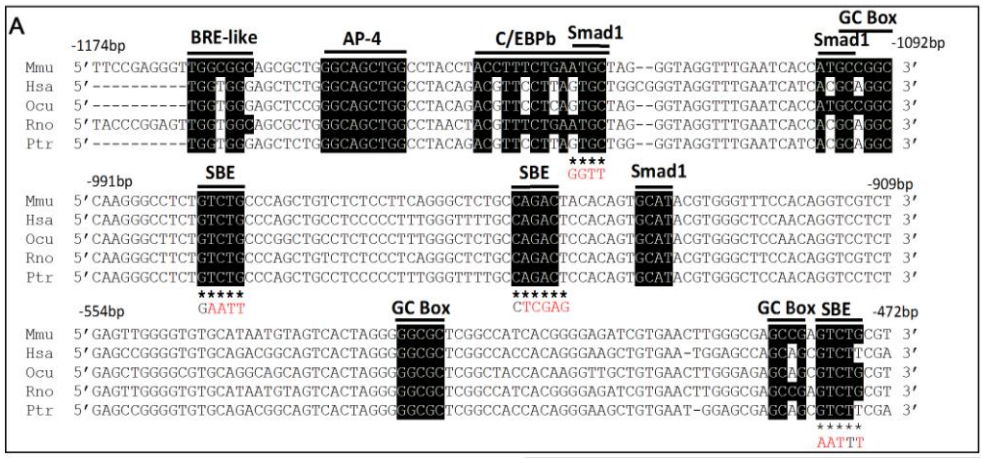

Figure. 6 Transcription modulation of *Vegfa* by Smad. A: Putative TF binding sites by Smad in *Vegfa* 5' upstream sequence. Mutations introduced in luciferase reporter assay are shown in red. B: Relative positions of ChIP primers in *Vegfa* chromatin are shown in arrows. s1: Smad1 binding motif, SBE: Smad binding element. C: *in vivo* ChIP indicates the bound of Smad to *Vegfa* chromatin. DNA from wild type OFT was immunoprecipitated with antibody against Smad1/5/8. Non-specific rabbit IgG were used as negative control. Unimmunoprecipitated DNA (10% input) was used as positive control. Each sample was analyzed with PCR amplification using primer sets shown in panel B. ddH_2O represents the PCR analysis in absence of template DNA. Bar graph on the right is ChIP-qPCR, showing percent input of IgG and anti-Smad. Each sample is triplicate. Error bars represent SEM. D: Native and mutated *Vegfa* reporter constructs. E: Luciferase assay. Native and mutated *Vegfa* reporter constructs were transfected with or without Ca-Alk3 construct. *=0.011, **=0.009. Error bars represent SEM.

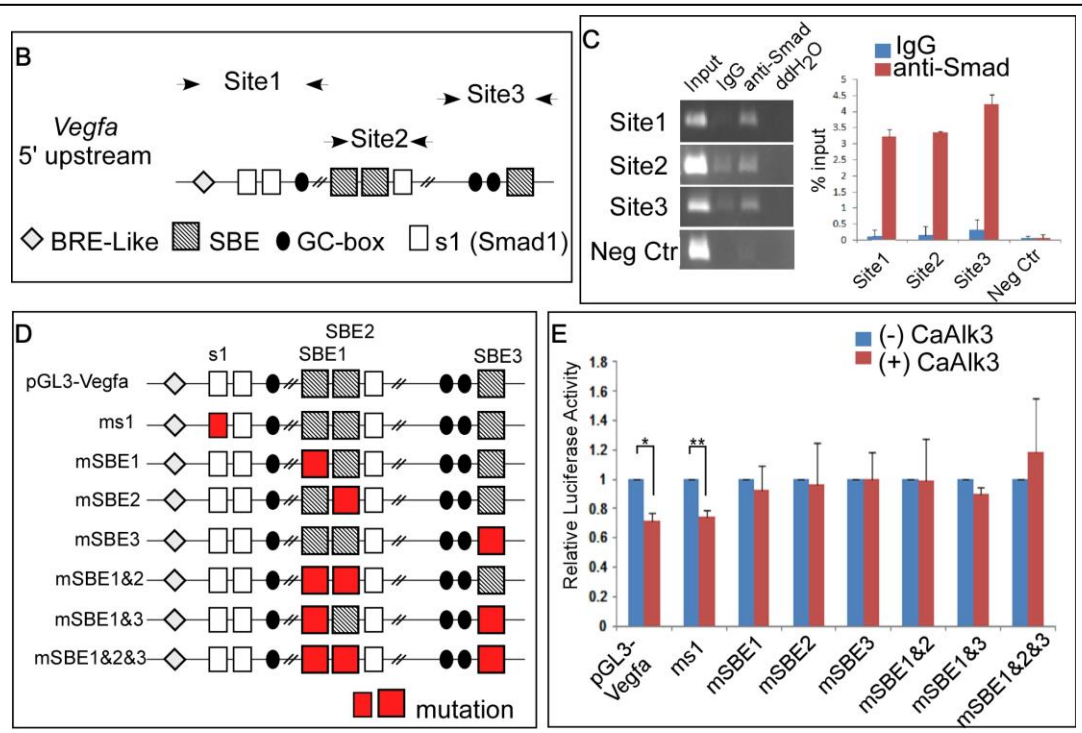

Figure 6 Continued.

To further determine if Smad directly regulated *Vegfa* transcription, we cloned approximately 1500 bp upstream of *Vegfa* and generated a luciferase reporter (Fig. 6D). To activate Smad-dependent Bmp pathway, we co-transfected a constitutive active form of the type 1 Bmp receptor Alk3, ca-Alk3 into p19 cell line (Wang et al., 2010). Luciferase assays demonstrated that *Vegfa* promoter activity was significantly diminished by 35% in the presence of ca-ALK3 (Fig.6E). To demonstrate if *Vegfa* promoter repression was due to direct Smad binding, we introduced mutations in the predicted Smad binding sites (Fig. 6D). Mutations in SBE1, 2, and/or 3 resulted in loss of repression activity by Bmp signaling (Fig. 6E), showing that Smad directly binds these sites and represses *Vegfa*. Mutation in s1 did not change luciferase activity (Fig. 6E), indicating that this motif may not be necessary in repressing *Vegfa*. The results indicated that Smad can directly repress *Vegfa* transcription, however, by only 35%. Since loss of *Bmp4/7* resulted in 175% increase in *Vegfa* levels, there may be other important Smad elements that are excluded from our luciferase reporter or other Bmp downstream effector mechanisms that contribute to *Vegfa* regulation.

MiR-17 and -20a are downstream effectors of Bmp in *Vegfa* repression

Our results raise the possibility that *Vegfa* levels are regulated by mechanisms other than direct Smad-binding to *Vegfa* chromatin. Alternative downstream Bmp effectors are microRNAs, which are involved in refinement of gene expression. *miR-17-92* is downstream of Bmp pathway in cardiac development (Wang et al., 2010). Bioinformatic analysis predicted a highly conserved *miR-17/20a* binding site in 3'UTR of *Vegfa* (Fig. 7A). The levels of *pri-miR-17-92* and mature *miR-17/miR-20a* were

decreased in the OFT of *Bmp4/7* dCKO embryos (Fig. 7B), showing that *miR-17/miR-20a* were downstream of Bmp4/7.

To determine the role of *miR-17-92* during OFT development, we analyzed *miR-17-92*$^{N/N}$ embryos. At E10.5 (Fig. 7C, D), *miR-17-92*$^{N/N}$ embryos showed OFT defects including lack of mesenchymal cushion formation. In both proximal and distal OFT, *miR-17-92*$^{N/N}$ embryos developed no mesenchymal cells, resembling the phenotype of *Bmp4/7* dCKO. At E14.5, *miR-17-92*$^{N/N}$ exhibited DORV phenotype, together with abnormal semilunar valve and VSD (Fig. 7E-F). Notably, loss of *miR-17-92* resulted in 1.7-fold increase in the level of *Vegfa* (Fig. 7G). This up-regulation of *Vegfa* was similar to what was observed in *Bmp4/7* dCKO (Fig. 7O). Taken together, our results suggest that *miR-17-92* is downstream of Bmp signaling during EMT process in OFT.

To determine if *Vegfa* can be regulated by *miR-17* and *-20a*, we cloned 1874 bp native *Vegfa* 3'UTR and constructed luciferase reporter vector (Fig. 7H). Co-transfection with *miR-17/20a* resulted in suppression of *Vegfa* 3'UTR reporter (Fig. 7I), while *miR-92a* did not suppress the luciferase activity. Then we mutated *miR-17/20a* binding site of *Vegfa* 3'UTR (Fig. 7H). Suppression by both *miR-17* and *-20a* was abolished in mutated *Vegfa* reporter (Fig. 7I), showing that the putative *miR-17/20a* site was responsible for 3'UTR silencing of *Vegfa*. The results strongly suggest that *miR-17/20a* are downstream effectors of *Bmp4/7* in repression of *Vegfa*.

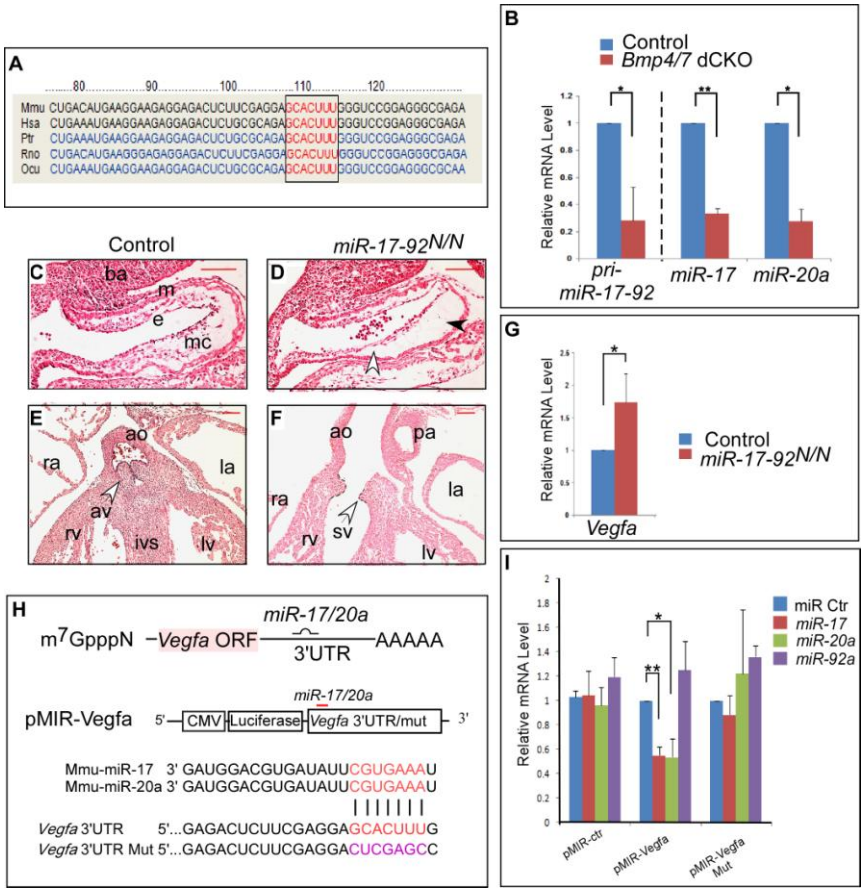

Figure. 7 *miR-17/20a* are downstream effectors of Bmp signaling. A: Analysis of *Vegfa* 3'UTR reveals a highly conserved *miR-17/20a* binding site. Mmu: mouse, Hsa: human, Ptr: chimpanzee, Rno: rat, Ocu: rabbit. B: qRT-PCR analysis of *pri-miR-17-92*, *miR-17* and *miR-20a* in the OFT of *Bmp4/7* dCKO embryos. *=0.049, **=0.027. Error bars represent SEM. (Control *n*=5, mutant *n*=3) C-F: Histological analysis on *miR-17-92* null embryos at E10.5 (C, D) and E14.5 (E, F). Black arrowheads show proximal EMT defect at E10.5 (D). White arrowheads show distal EMT defect (D) and abnormal semilunar valve at E14.5 (F). ba: branchial arch; m: myocardium; mc: mesenchymal cushion; e: epithelium; ao: aorta; pa: pulmonary artery; la: left atrium; ra: right atrium; lv: left ventricle; rv: right ventricle; av: aorta valve; sv: semilunar valve; ivs: interventricular septum G: qRT-PCR analysis of *Vegfa* in the OFT of *miR-17-92* mutant. For each qRT-PCR (control *n*=4, mutant *n*=4), *P*-value was analyzed by t-test (two-tailed). *=0.046. Error bars represent SEM H: (Top) *miR-17/20a* seed sequences on *Vegfa* 3'UTR. (Middle) miR luciferase reporter construct. (Bottom) Mutation of seed sequences. I: Luciferase assay. The assay was performed by transfecting reporter construct and *miR-17 or -20a*. *miR-92a* was used as a negative control. *P*-value was analyzed by t-test (two-tailed). *=0.032, **=0.009. Error bars represent SEM.

Repression of Vegfa regulates EMT process during OFT development

Vegfa inhibits mesenchymal transformation in the AV cushion (Chang et al., 2004), however, the potential roles of Vegfa in EMT process during Bmp-mediated OFT development have not been investigated. To determine if Bmp regulate EMT through *Vegfa* repression, we investigated if reducing Vegfa can rescue EMT caused by *Bmp4/7* deletion. We performed *ex vivo* analysis by culturing the OFT from E10.5 embryos on collagen gel, with the endocardium exposed to the gel (Fig. 8A). In control explants, a halo of mesenchymal cells formed around the myocardium, with non-invasive mesenchymal cells on the surface of gel and invasive mesenchymal cells invading the collagen depths (Fig. 8B, C). In the OFT of *Bmp4/7* dCKO, both invasive and noninvasive EMT were absent (Fig. 8D, E). Administration of sFlt, a soluble Vegfa antagonist, partially suppressed mesenchymal transformation defect in *Bmp4/7* dCKO by rescuing the non-invasive mesenchyme cells formation (Fig. 8F). Invasive EMT was not rescued by antagonizing *Vegfa* (Fig. 8G), suggesting this process is regulated by other downstream Bmp targets, such as *Snail*.

Next, to determine if *miR-17* and *20a* regulate EMT through *Vegfa* regulation, we performed explant culture from *miR-17-92*$^{N/N}$ OFT (Fig. 8H, I). The OFT from *miR-17-92* null lacked both invasive and noninvasive EMT (Fig. 8H, I), which recapitulated the explant from *Bmp4/7* dCKO (Fig. 8D). After addition of the *Vegfa* antagonist sFlt to the explant, both non-invasive and invasive EMT process was rescued in the miR-17-92 n/n explants (Fig. 8J, K), showing that *Vegfa* down-regulation was sufficient to rescue *miR-17-92* loss of function phenotype. Since antagonizing *Vegfa* was not sufficient to

rescue invasive EMT in the explant from *Bmp4/7* (Fig. 8G), regulation of *Vegfa* by *miR-17-92* was one of multiple downstream effectors of Bmp signaling.

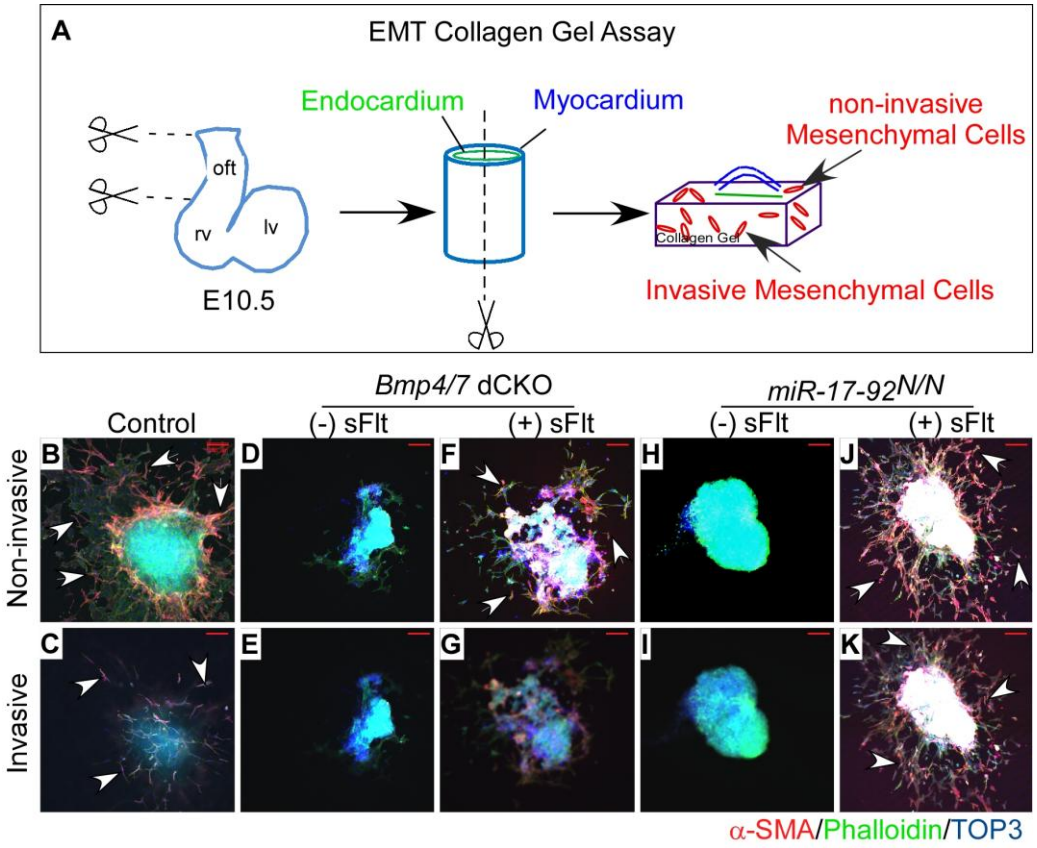

Figure. 8 *Ex vivo* collagen gel assay of the OFT. A: Diagram illustration of the OFT explant culture on collagen gel. The OFT from E10.5 embryo was dissected, cut, and placed on the collagen gel. Inner endocardium layer (shown in green) was exposed to the gel, with myocardium (shown in blue) on the top. B-K: EMT assays on the OFT of control, *Bmp4/7* dCKO, and *miR-17-92* null embryos. EMT was visualized by Phalloidin to outline the cell shape and by alpha-SMA immunostaining to stain mesenchymal cells. TOP3 was used to stain nuclei. Invasive EMT is observed on the surface of collagen gel, (Top panels, Arrows) and non-invasive EMT is observed in the gel (Bottom panels, Arrowheads). Scale bar=100 μm.

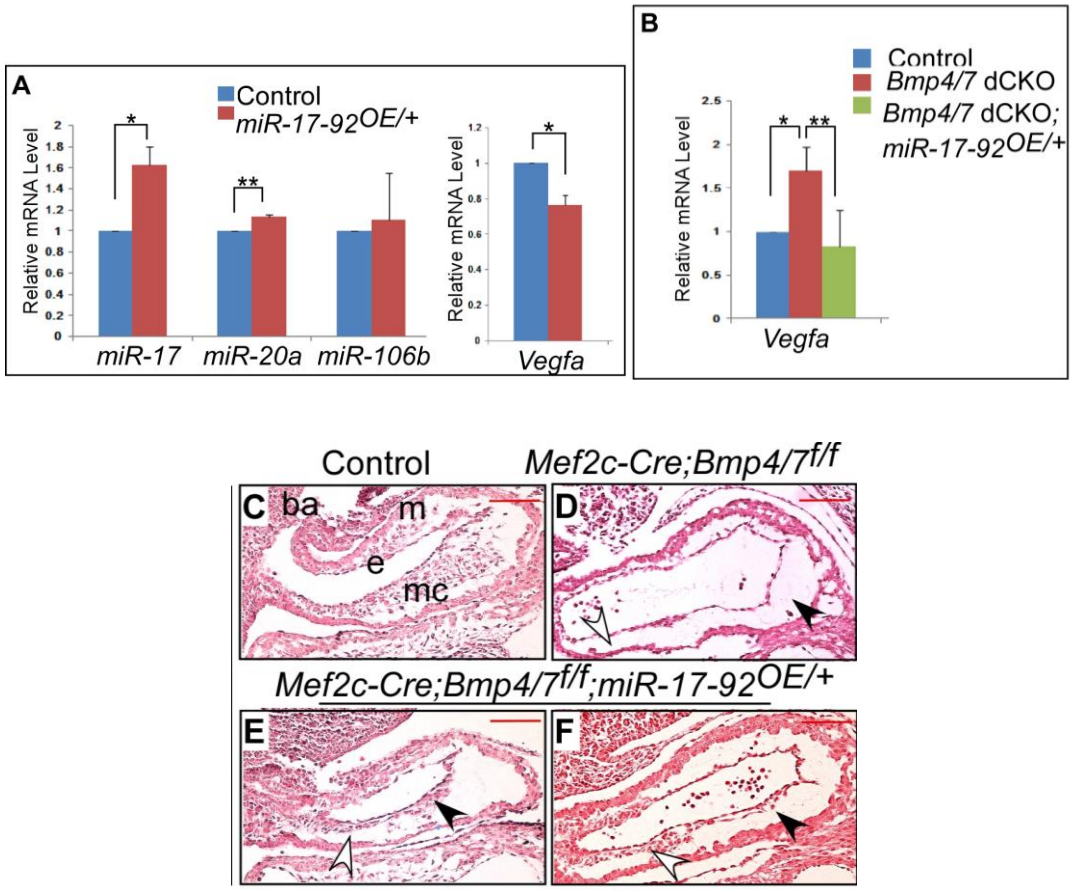

Figure. 9 Rescue of *Bmp4/7* deficiency by conditionally overexpressing *miR-17-92*. A: qPCR analysis on *miR-17*, *20a* and Vegfa on the OFT of *miR-17-92*$^{OE/+}$ embryos. *miR-106b* is used as negative control. *=0.016, **=0.033, (Control *n*=4, mutant *n*=4) Expression of *Vegfa* in *miR17-92*$^{OE/+}$ embryos. *=0.047. B: qRT-PCR analysis of Vegfa on *Bmp4/7* dCKO and *miR17-92*$^{OE/+}$ (Control *n*=6, Bmp4/7 mutant n=5, mutant *n*=3). *p*-value was analyzed by t-test (two-tailed). *=0.045, **=0.048. Error bars represent SEM. C-F: Histological analysis on the embryos of *Bmp4/7* dCKO and *miR-17-92* overexpression OFT at E10.5. Black arrowheads show proximal OFT mesenchymal cells, white arrowheads point distal OFT mesenchymal cells. ba: branchial arch; m: myocardium; mc: mesenchymal cushion; e: epithelium; Scale bar=100 μm.

MiR-17-92 can rescue defects in EMT caused by loss of Bmp

To address the hypothesis that *miR-17/20a* are direct downstream effectors of Bmp in EMT process *in vivo*, we overexpressed *miR-17-92* in the Bmp4/7 dCKO by crossing *miR-17-92*$^{OE/+}$ (Xiao et al., 2008) and *Mef2c-Cre* lines. qRT-PCR data showed that *miR-17* and *miR-20a* were mildly elevated by approximately 1.3 fold in the OFT of *Mef2c-Cre*;*miR-17-92*$^{OE/+}$ (Fig. 9A). *Vegfa* levels were also moderately down-regulated in the OFT of *Mef2c-Cre*;*miR-17-92*$^{OE/+}$ (Fig. 9A), demonstrating that *miR-17-92* repressed *Vegfa in vivo*. To determine if *miR-17-92* can compensate for the loss of *Bmp4/7*, we generated *Mef2c-Cre*;*Bmp4/7*$^{f/f}$;*miR-17-92*$^{OE/+}$ embryos. Mesenchymal cushion formation was observed in the OFT of *Mef2c-Cre*;*Bmp4/7*$^{f/f}$;*miR-17-92*$^{OE/+}$ embryos (Fig. 9E-F): proximal cushion-forming cells were observed in 83% of the embryos while distal cushion cells were observed in all embryos (Table 2). At E14.5, the valve defect of *Bmp4/7* dCKO embryos was rescued by overexpression of *miR-17-92*, while OFT septation was partially rescued in distal part (data not shown). The level of *Vegfa* in *Mef2c-Cre;Bmp4/7*$^{f/f}$*;miR-17-92*$^{OE/+}$ was decreased compared to *Mef2c-Cre;Bmp4/7*$^{f/f}$ and comparable to that of control embryos (Fig. 9B), suggesting that suppression of *Vegfa* by Bmp was mediated by *miR-17* and *20a*. These results strongly suggest that *miR-17* and *20a* are downstream effectors of Bmp signal during OFT development.

Table 2 OFT phenotype in *Bmp4/7* mutant

	OFT mesenchyme present	
Genotype	Proximal OFT	Distal OFT
Mef2c-Cre;Bmp4/7$^{f/f}$	1/17	6/17
Mef2c-Cre;Bmp4/7$^{f/f}$;miR17-92$^{OE/+}$	5/6	6/6

Although cushion formation was observed in *Mef2c-Cre;Bmp4/7$^{f/f}$;miR-17-92$^{OE/+}$* embryos, mesenchymal cushion-forming cells were fewer in the rescued embryos indicating partial suppression (Fig. 9C-F). In addition, the extent of mesenchymal cushion formation was variable (Fig. 9C-F, Table 2). Together these data support the hypothesis that Bmp signals are mediated by the other effector mechanisms in addition to *miR-17*.

Discussion

Our data uncover a direct interaction between the Bmp and Vegfa signaling pathways important for normal OFT development. Moreover, our findings uncover a mechanism to tightly modulate Vegfa activity levels in OFT. Our results also provide new insight into the mechanism for coordinated development of CNC and endocardial cells as they contribute to the conotruncal cushions. Lastly, our data reveal that *miR-17-92* indirectly, via non-autonomous mechanisms, regulates cardiac neural crest development in addition to SHF derived tissues.

Coordinated regulation of cushion formation derived from multiple cell types

The conotruncal cushions are derived from both CNC and the endocardium. Bmp-signaling has been implicated previously in EMT within the atrioventricular canal AVC. We now show that Bmp-signaling is also important for EMT within OFT. Previous data in the AVC indicate that Bmp regulates genes such as *Twist* and *Snai1* to promote EMT and while we did not focus on that mechanism here, it is likely that similar mechanisms are at work in both OFT and AVC. Our finding that Bmp signaling negatively regulates Vegfa in OFT provides important insight into the coordinated regulation of the OFT cushions. In the OFT, in contrast to AVC, there are three separate tissues developing in close proximity: myocardium, endocardium, and CNC. We provide evidence that the *Bmp-miR-17-92* mediated *Vegfa* repression is a critical mechanism to ensure coordinated OFT development.

The importance of Vegf signaling in endocardium has recently been shown. Deleting the Vegf receptor, *Neuropilin 1*, in endocardial cells disrupts OFT development

with abnormal cushion morphogenesis (Zhou et al., 2012). This finding indicates that endocardium is a target cell for Vegf signaling. There are no previous findings implicating Vegfa signaling in CNC development. Our data suggest that elevated Vegfa inhibits CNC influx into the OFT, however, more experiments are required to definitively make this conclusion.

A mechanism to tightly modulate Vegfa activity in the developing heart

Previous genetic studies have shown that Vegfa dose must be maintained within a narrow window for normal embryonic development. Vegfa heterozygosity, with reduced dosage, as well as small gains in Vegfa activity result in defective embryonic development. Loss of a single *Vegfa* allele is embryonic lethal at mid-gestation due to impaired angiogenesis and blood-island formation (Ferrara et al., 1996). Moreover, there are cardiomyoblast differentiation defects in *Vegfa* heterozygotes. Haigh et al. found that heterozygous inactivation of *Vegfa* using *Collagen2a1-Cre* caused embryonic lethality at E10.5 with defects in myocardial and endocardial layers of the heart (Haigh et al., 2000). A different *Vegfa* allele, $Vegf^{\delta^o}$, results in a three-fold overexpression of *Vegfa* during development. Heterozygotes for this allele are viable, however, homozygous embryos die at E9.0 with dorsal aortae defects and severe abnormalities in yolk sac vasculature (Damert et al., 2002).

Our data indicate that in the OFT, Vegfa activity is concurrently regulated by Smad transcriptional repression and post transcriptional repression by miRs. Vegfa has been previously reported to be regulated by miRs, including the *miR-17* family, in other contexts including cultured breast cancer cells and diabetes (Cascio et al., 2010; Long et

al., 2010). However, our finding that miR regulation cooperates with Smad mediated repression provides new insight into the mechanisms underlying tight *Vegfa* dosage regulation.

Bmp interacts with Calcineurin-NFAT signaling

Previous work indicated that NFATc1 mutants have conotruncal valve phenotypes similar to *Mef2c-cre;Bmp 2,4,7* triple mutant (Y. Bai and J. Martin, in preparation). Moreover, similar to what we have discovered for Bmp-signaling, NFATc1 inhibits *Vegfa* expression in the E9.5 OFT to permit EMT (Chang et al., 2004; Stankunas et al., 2010). NFATc1 expression was reduced in the AV cushion endocardium of Bmp2 conditional mutant embryos (Ma et al., 2005). There is evidence from pulmonary vascular cells that NFAT and Bmp are in a linear genetic pathway (Chan et al., 2011). Other intriguing data indicate that NFAT can promote chondrogenesis in vitro, a known function for Bmp-signaling (Tomita et al., 2002). More work will be required to investigate potential interactions between NFAT-calcineurin and Bmp signaling in the developing OFT.

Summary

Congenital heart disease (CHD) is a common and devastating anomaly that affects approximately 1% of live births. Defects of the outflow tract make up a large percentage of human CHD. We investigated Bmp (Bone morphogenetic protein) signaling in outflow tract (OFT) development by conditionally deleting both *Bmp4* and *Bmp7* in second heart field (SHF). SHF *Bmp4/7* deficiency resulted in defective endothelial to mesenchyme transition (EMT) and reduced cardiac neural crest (CNC) ingress with resultant persistent truncus arteriosus (PTA). Using a candidate gene approach, we found that vascular endothelial growth factor A (*Vegfa*) was upregulated in the *Bmp* mutant hearts. To determine if *Vefga* is a downstream Bmp effector during EMT, we examined if *Vegfa* is transcriptionally regulated by the Bmp receptor-regulated Smad. Our findings indicate that Smad directly binds to *Vegfa* chromatin and represses *Vegfa* transcriptional activity. We also found that *Vegfa* was a direct target for *miR-17-92* cluster that is also regulated by Bmp signaling in SHF. Deletion of *miR-17-92* reveals similar phenotypes as loss of *Bmp4/7* SHF deletion. To directly address the function of *Vegfa* repression in *Bmp* mediated EMT, we performed *ex vivo* explant cultures from *Bmp4/7* and *miR-17-92* mutant hearts. EMT was defective in explants from *Bmp4/7* dCKO (*Mef2c-Cre;Bmp4/7*$^{f/f}$) and *miR-17-92* null. By antagonizing Vegfa activity in explants, EMT was rescued in *Bmp4/7* dCKO and *miR-17-92* null culture. Moreover, overexpression of *miR-17-92* partially suppressed the EMT defect in *Bmp4/7* mutant embryos. Together, our study unveils that *Vegfa* levels in OFT are tightly controlled by Smad- and miR-dependent pathways to modulate OFT development (Fig. 10).

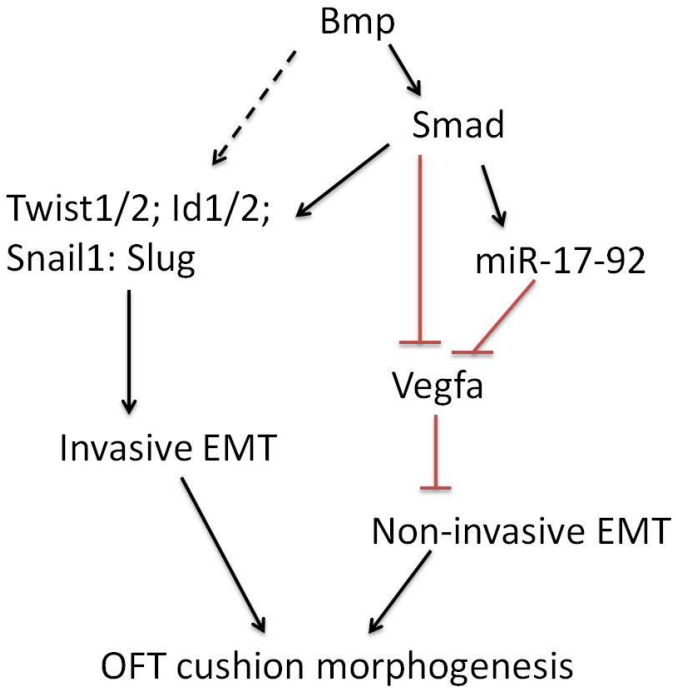

Figure 10. Molecular mechanism on *Bmp* regulation of OFT development. Bmp signals regulate EMT related genes such as Twist1/2, Id1/2, snail1 and slug, to promote invasive EMT. In addition, Bmp control vegfa expression by Smad and miR mechanisms to regulate non-invasive EMT. All together are important for the normal OFT cushion morphogenesis

CHAPTER III

BMP SGINALING DISRUPTION IN SECOND HEART FIELD IMPAIRS AORTA DEVELOPMENT AND EARLY ONSET OF AORTA ANEURYSM

Background and Significance

Marfan syndrome (MFS) is a heritable connective tissue disorder that occurs at 1 individual per 3000-5000 in the population. It's first described by Antoine Marfan a French pediatrician in 1896 and well known for its classic physical features such as pectus excavatum, lens ectopia, arachodactyly, and tall stature. MFS is widely reported because of aortic root dilation and dissection, which is the major cause of mortality in this population (Jain et al., 2011; Milewicz et al., 2008; Neptune et al., 2003). Lack of cure for MFS, the syndrome is treated by preventive medication to slow progression of aortic dilation or surgical replacement of the aorta (Groenink et al., 2013; Mirick et al., 2013).

Fibrillin-1 (Fbn-1) is one of the genes identified as linked to MFS (Dietz et al., 1991). Fbn-1 locus encodes a 350-kDa glycoprotein fibrillin-1, which is essential for the proper formation of extracellular matrix (ECM). It has a "beads-on-a-string" structure when viewed by electron microscope (Dietz and Pyeritz, 1995). Fbn-1 protein is pivotal for structural integrity of the microfibrils which provide a scaffold for elastic fibers (Yanagisawa and Davis, 2010), and also serves as a reservoir for growth factors such as Tgf-β and BMP to modulate their bioactivity (Nistala et al., 2010). Interaction between Tgf-ß signaling and Fibrillin-1 has been well described. After it is synthesized, Tgf-β

ligand forms homodimer and interact with a latency associated peptide (LAP) to form a complex called small latent complex (SLC). SLC is then binds to latent Tgf-β-binding protein (LTBP) to form large latent complex (LLC) to be secreted to the ECM. Fbn-1 protein can bind LLC to control the levels of Tgf-β signal. Mutation in Fbn-1 causes malfunction of sequestering Tgf-β by releasing LLC in the ECM, thus results in increased activity of Tgf-β ligands (Neptune et al., 2003). Increased level of Tgf- ligands in the ECM then causes increased Tgf-β signaling in surrounding cells, detected as increased phosphorylation level of the downstream target Smad2 (pSmad2).

Non-canonical Tgf-β signal pathway is also associated with MFS (Holm et al., 2011). Activation of Jun N-terminal kinase-1 (JNK-1) is detected in Smad4-deficient MFS mice ($S4^{+/-}$, mice harboring a deletion of exon 8 of the Smad4 gene) (Holm et al., 2011), but a JNK antagonist attenuated aortic growth without retained full Smad4 expression. Losartan is a blocker for angiotensin II type I, and it is known to suppress the expression of Tgf-β ligands. Treatment of losartan can achieve some rescue by reduction of ERK1/2 activation (Holm et al., 2011).

Genes encoding smooth muscle actin are associated with MFS. The vascular smooth muscle cells (SMCs) are the major cell component of aorta media and functions as contract machinery to regulate pulse pressure and blood flow. In addition, SMCs function as a mechanistic sensor to monitor the biomechanical force. Alternations of SMC proteins including ACTA2 and MYH11 cause aorta aneurysm (Milewicz et al., 2008), which is caused by activation of SMC repair pathways through activation of MMP and renin-angiotensis system.*Tgbr2* mutation lead to decreased expression of

SMC contractile protein which contribute to the pathogenesis of aneurysm (Inamoto et al., 2010). SMC-specific ablation of *Tgfbr2* resulted in impaired elastogenesis and aneurysm in mice embryos which was prone to dilation and aneurysm (Choudhary et al., 2009).

More recently miR has been studied in relation with ECM and aortic aneurysm. miR is a small non-coding RNA molecule (~22 nucleotides) found in plants and animals. They can orchestrate gene expression profiles associated with phenotype and disease. miR-29, which is a Tgf-β-responsive miR, has been identified to play a important role during aortic development and aging. This family (miR-29a/b/c) has been studied to target genes that encode ECM proteins including collagen genes such as CoL1A1, CoL1A2 and CoL3A1; Fbn-1, and elastin (ELN) (van Rooij et al., 2008). Reduction of miR-29b in the aortic wall can ameliorate abdominal aortic aneurysm (AAA) progression in pancreatic elastase (PPE) infusion model in C57BL/6 mice and AngII infusion model in Apoe-/- mice (Maegdefessel et al., 2012). However, the increased level of miR-29b is not detected in mouse model of TAA (Thoracic aorta aneurysm) and human TAA tissue.

BMP is a member of Tgf-β superfamily and its signal is transduced through a canonical pathway involving phosphorylation of Smad1/5/8 by the ligand-receptor complex (Bai et al., 2013). Upon binding with Smad4, pSmad1/5/8-Smad4 complex shuttles from cytoplasm to nucleus and function as transcriptional factor, either activator or suppressor (Kawabata et al., 1998; Zwijsen et al., 2003). BMP is also associated with regulation of miR transcription. miR-17-92 is reported to be a downstream target of

BMP signal pathway to regulate OFT development and differentiation (Bai et al., 2013; Wang et al., 2010).

Although little evidence is revealed about the interaction of BMP and Fbn-1, studies show that mice deficient in both Fbn-1 and Fbn-2 exhibit PTA, which is found in the mice with loss of BMP and Tgf-β signaling. In addition, in the developing autopad, Fbn-2 deficient mice show loss of Bmp7 and recapitulate the syndactyly phenotype observed in Bmp7 mutant mice (Arteaga-Solis et al., 2001). Like it controls Tgf-β activity, Fbn-1 controls the bioactivity of BMP ligands in the ECM during bone formation (Nistala et al., 2010).

In this study, we found that loss of Bmp4 can exacerbate aortic phenotype including aorta aneurysm, collagen disposition and elastic fragmentation in adult. During development, BMP directly regulates Fbn-1 associated with regulation of Tgf-β signal pathway. Loss of BMP results in smooth muscle cells in the aorta to fail to terminally differentiate. Furthermore, miR-17-92 overexpression can compensate the abnormality caused by loss of BMP signal, including suppression of sarcomeric actin expression and Tgf-β activation. Here we first identified that BMPsignaling plays an important role in aorta aneurysm development and shed a light on the underlying molecular mechanism of MFS, providing potential treatment targets for the clinical trial.

Material and Methods

Mouse lines

The *Bmp4* flox, *miR-17-92* null and *miR-17-92*^{OE} alleles and *Mef2c-Cre* lines have been previously described (Liu et al., 2004; Ventura et al., 2008; Verzi et al., 2005; Xiao et al., 2008). Bmp7 flox mice have been described earlier (See A-1(Bai et al., 2013)). *miR- 17-92* LacZ transgenic mice is previously described (Wang et al., 2013). Fbn-1$^{C1039G/+}$ lines have been previously described (Bai et al., 2013; Judge et al., 2004; Liu et al., 2004; Ventura et al., 2008; Verzi et al., 2005; Xiao et al., 2008).

β-galactosidase staining, histology and imaging

Embryos were fixed overnight in buffered formalin, dehydrated through graded ethanol, and paraffin embedded. Sections were cut at 7 μm and stained with H&E. detection of LacZ expression on whole embryos was performed as previously described (Lu et al., 1999).

Adult hearts were dissected from animal and fixed in 4% paraformaldehyde (PFA) overnight at 4˚C. Samples are transfer to 70% ethonal for dissection and storage, then dehydrated through graded ethanol, paraffin embedded, and sectioned. Sections were stained for standard stains including Russell-Movat pentachrome stain, or Masson's Trichrome staining.

Whole mount image were taken by Zeiss Stereomicroscope. Slides images were taken by Nikon microscope.

Immunofluorescence staining

Immunofluorescence analysis were performed on either frozen or paraffin sections. For frozen section, embryos were embedded in OCT, snap freezed and sectioned to 8 μm on Superfrost/Plus Slides (Fisher Scientific, Pittsburgh, PA). After air dry for 10 mins, slides were fixed in cold acetone for 10 mins, followed by 4 mins rehydration in PBS at room temperature.

For paraffin section, embryos were fixed in 4% PFA, dehydrated, embedded in paraffin and cut to 7 μm sections. The antigens were retrieved by incubating in 10 mM citrate buffer for 20 mins at 100℃ or as suggested by manufacturers of the antibodies.

Fbn-1 antibody is courtesy of Dr. Lynn Sakai (Oregon Health & Science University). The source and concentration of primary antibodies are α-SMA-Cyan3 (1:100; Sigma-Aldrich), anti-MF20 (1:200; Developmental Studies Hybridoma Bank), anti-Isl1 (1:200; Developmental Studies Hybridoma Bank), p-Smad2 (1:200; Cell signaling #9510). HRP-conjugated secondary antibody (Bio-Rad Co., Hercules, CA) was used and visualized using TSA™ plus Fluorescence Systems from PerkinElmer (Boston, MA), or Alex Fluor® 488 Goat anti-rabbit IgG(H+L) (1:500; Invitrogen A-11008) was used. Nuclei were stained with Dapi (invitrogen). Images were taken by Zeiss LSM 510 meta confocal microscope.

***In vivo* chromatin immunoprecipitation and ChIP-PCR**

Approximately 40 aorta of E14.5 wild type mouse embryos were dissected and followed by the chromatin immunoprecipitation (ChIP) analysis. Soluble chromatin was prepared after formaldehyde crosslinking and sonication by Bioruptor. Smad1/5/8

antibody (sc-6031 X, Santa Cruz) was used to immunoprecipitate protein-bound DNA fragments. Rabit IgG was used as control. Primers designed for irrelevant chromatin sequence to Smad were used as a negative control. SYBR Green was used for ChIP-qPCR and results were analyzed by fold change method (Invitrogen). Primer sequences are available in supplementary material Table S1.

Transthoracic echocardiography

Transthoracic echocardiography was performed on 2, 3. 10 month old Mef2c-Cre;$Bmp4^{f/+}$;$Fbn\text{-}1^{C1039G/+}$ and Control male mice ($Bmp4^{f/+}$).. Mice were anesthetized by 1.5% isoflurane inhalation and placed on a heated platform (37 ℃) with integrated physiological monitoring capabilities. Two-dimensional B-mode imaging was recorded using VisualSonics 770 system (Toronto, Canada) with a 30 MHz scanhead (RMV707B) to capture long axis projection with guided M-Mode and PW Doppler recorded. The average reading for each echocardiographic parameter was recorded from at least 3 distinct frames from each individual of the 2 experimental groups. Statistical significance was determined using Student's t-test ($p < 0.05$).

Results

BMP4 haploinsufficiency aggravates aorta aneurysm in *Fbn-1*$^{C1039G/+}$

To understand role of BMP in adult mice, we first examined Bmp4 expression using *Bmp4*^{LacZneo} mice (Bai et al., 2013; Bonilla-Claudio et al., 2012; Lawson et al., 1999; Selever et al., 2004; Wang et al., 2010). Bmp4 was consistently expressed in the coronary sinus, aorta, pulmonary artery and coronal vessels (A-4, A,B). Sections showed that Bmp4 was expressed in endothelium, media and smooth muscle of the aortic vessel, atrium-ventricular valves (Fig. 12A), but no signal was detected in the aorta valve (data not shown). Expression of Bmp4 in adult suggests it may have function in adult.

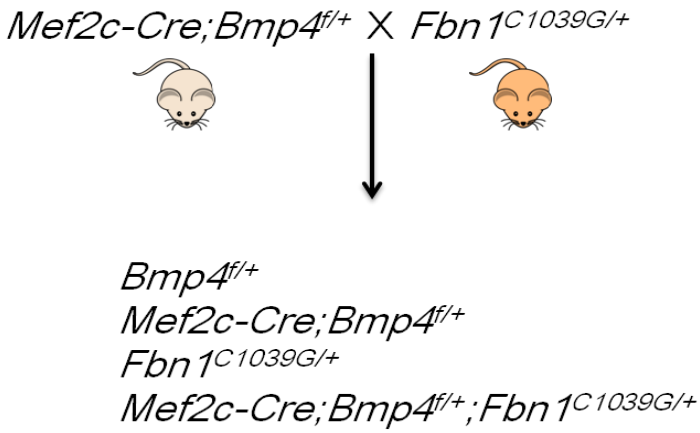

Figure 11. Study strategy for Bmp function assay on aorta. To study the roles of Bmp on aorta maintenance, *Mef2c-Cre;Bmp4*$^{f/+}$ is crossed with mice carry *Fbn1*$^{C1039G/+}$, progeny with different genotype are examined as indicated.

To determine the role of BMP signaling in Marfan syndrome, we examined the roles of BMP in adult aorta. Since homozygous mutant of Bmp4 does not survive till adulthood, we analyzed combined heterozygous of Bmp4 and Fbn-1$^{C1039G/+}$(*Mef2c-Cre;Bmp4$^{f/+}$;Fbn-1$^{C1039G/+}$*, *Bmp4;Fbn-1* dHet for short, Fig. 11). *Mef2c-Cre*, which delete genes in the lineage contributes to outflow tract, was used for our study. To examine aorta aneurysm, we measured diameter of the aorta root visualized by echocardiography analysis at 2, 3 and 10 month-old mice. *Bmp4;Fbn-1* dHet shows more severe aortic aneurysm than *Fbn-1$^{C1039G/+}$* mice (Fig.12B), with significant increase of aorta dimension as early as 2 month old (Fig. 12C).

At 10 months, *Bmp4;Fbn-1* dHet mutants exhibit aorta dilation. We found severe aneurysm in *Bmp4;Fbn-1* dHet mutants in gross level at 10 months, with different penetration. Histological analysis reveals the aorta morphology of 10 month-old mice.

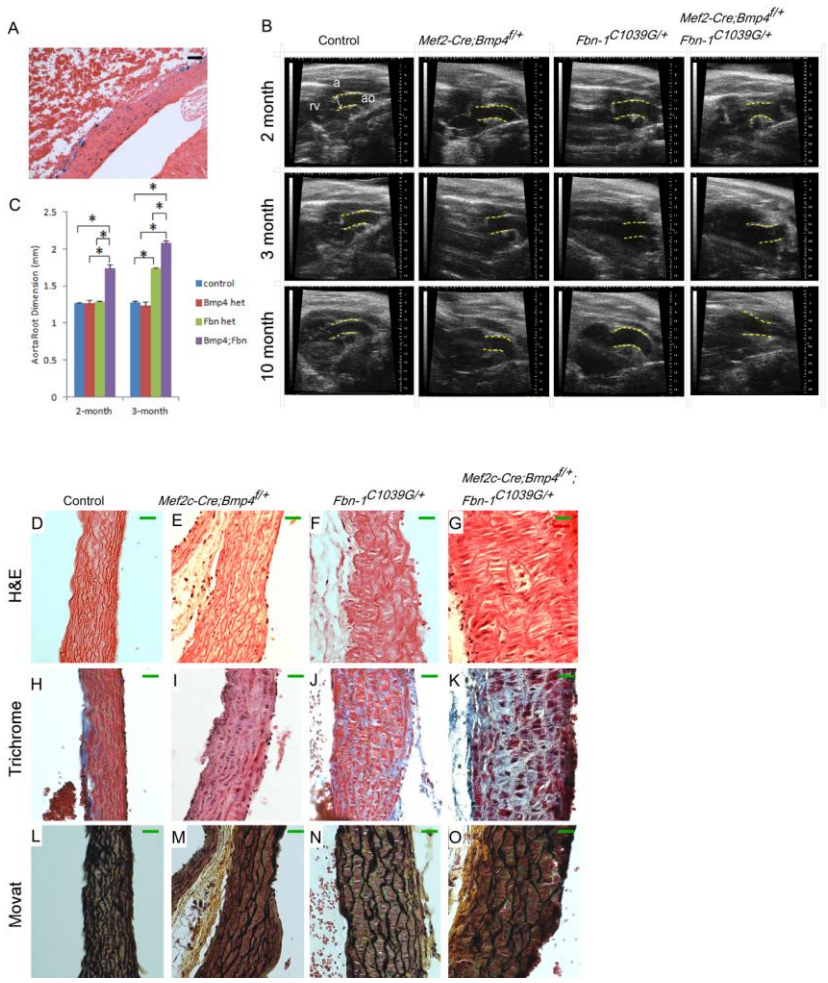

Figure 12. Haploinsufficiency of Bmp exacerbates aorta aneurysm in Fbn-1$^{C1039G+/-}$ mice. Adult animals of control (Bmp4$^{f/+}$), BMP4 het (Mef2c-Cre;Bmp4$^{f/+}$), Fbn het (Fbn-1$^{C1039G/+}$), and BMP4; Fbn dHet (Mef2c-Cre;Bmp4$^{f/+}$;Fbn-1$^{C1039G/+}$) were analyzed for aorta aneurysm. A: Expression of Bmp4 examined by LacZ staining. scale bar =50 μm. B: Echocardiography analysis on 2, 3, 10 month-old adult mice. Distance between yellow dotted line were measured (arrow). a: atrium, ao: aorta, rv: right ventricle. C: Aorta dimension of 2 and 3 month old mice. Aorta dimension is measured by Image J software from echoed mice, each mice were measured at 3 times and average is used for statistical analysis. p-value is analyzed by t-test (two tailed). * P<0.05. D-O: Histological analysis on 10 months old aorta of the control (D, H, L), BMP4 het (E, I, M), Fbn-1 het (F, J, N), and double het (G, K, O) mice. D-G: H&E staining. H-K: Trichrome staining. Collagen is stained blue, nuclei is stained black, muscle, cytoplasm and keratin is stained red. L-O: Movat staining. Nuclei and elastic fibres are stained black, collagen fibres are stained yellow, mucin is stained blue, fibrin is stained bright red, and muscle is stained red. Scale bar (green)=50 μm (D-O).

H&E staining showed that *Bmp4;Fbn-1* dHet mice had thicken media and abnormal smooth muscle cells with elongated cell shape in the aorta (Fig.12D-G). We found increased collagen deposition indicated in blue staining in *Fbn-1*$^{C1039G/+}$ compare to control, and more collagen deposition was detected in *Bmp4;Fbn-1* dHet visualized by trichrome staining (Fig.12H-K). In addition, we found disorganized and fragmented elastin fibers in Fbn-1^{C1039G} and the level of defect is more sever in *Bmp4;Fbn-1* dHet$^{/+}$ (Fig.12L-O). *Mef2c-cre;Bmp4*$^{f/+}$ mice also showed mild aortic phenotype compared to control (Fig.12D,H,L). Surprisingly, we found disrupted assembling of α-SMC in *Mef2c-cre;Bmp4*$^{f/+}$, as well as in *Fbn-1*$^{C1039G/+}$ and *Bmp4;Fbn-1* dHet (A-5). These results indicate that mice with BMP and Fbn-1 mutation were more prone to develop dilated aorta root even at young stage, with worse pathology aorta with aging which is likely to contribute to aorta aneurysm and rupture.

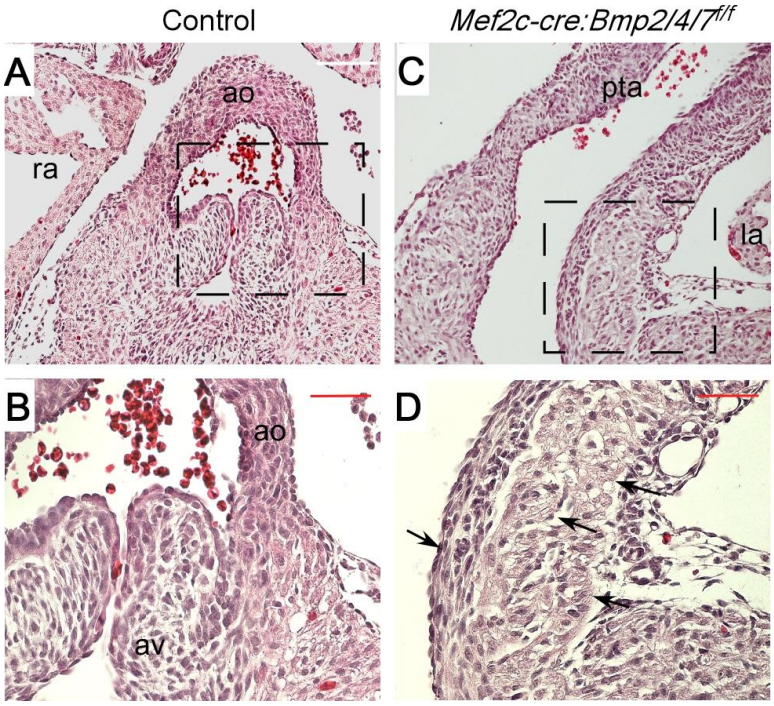

Figure 13. Bmp2/4/7 ablation results in OFT abnormality. A-D: Histological analysis on control (Bmp2/4/7$^{f/f}$) and Bmp2/4/7 CKO (Mef2c-Cre;Bmp2/4/7$^{f/f}$). E14.5 embryos were collected, sectioned, and stained for H&E for histological analysis. Panels B and D are zoomed-in images of panels A and C, respectively. Arrows show disorganized cells in the OFT. la: left atrium; ra: right atrium; ao: aorta; av: aorta vavle; pta: persistent truncus asteriosus. Scale bar (white)=100 μm; Scale bar (red)=500 μm.

Loss of BMP results in disorganized SMC in OFT

Our results show that aorta dilation occurs at very early age of Bmp4;Fbn-1 dHet, indicating Bmp4 regulates aorta formation in early stages or during development. Likewise in people, some patients with MFS develop severe aorta aneurysm in early childhood, indicating the disease is due to developmental defects. Thus, we determined the role of BMP in embryonic mouse model. To begin understating the roles of BMP in aorta, we examined its expression pattern during developmental stage. At E14.5, Bmp4 was expressed in aorta, pulmonary artery and coronary sinus (A-4, F,G). In contrast, Bmp2 was not detected at aorta at E14.5 (A-4, I,J) and adult mice (A-4, C,D), although Bmp2 was expressed in the OFT at early embryonic stage (Ma et al., 2005). However, Bmp2 was expressed in pulmonary artery throughout development (A-4, C,H). Whole mount hybridization demonstrated that Bmp7 was expressed in the whole heart loop during developmental stage (Bai et al., 2013). Thus, all three ligands potentially regulate aorta development.

Because of function redundancy of BMP ligands and overlapping expression of Bmp2, Bmp4, Bmp7 in the OFT during development, we crossed mice carrying *Mef2c-Cre* and *Bmp2/4/7* flox allele with mice carrying *Bmp2/4/7* flox/flox allele. *Bmp2/4/7* CKO (*Mef2c-Cre;Bmp2/4/7*$^{f/f}$) exhibited PTA phenotype (Fig.13C), consistent with previous studies (Bai et al., 2013). The single truncus showed aberrant morphology, including disorganization of the cells, dilated OFT root and thickened vessel wall (Fig.13C, D). Similar phenotype was observed in other combined ablation of BMP ligands (A-6, A-H). In addition, *Bmp2/4/7* CKO formed no valve, had small right

ventricle and ventricular septum defect (VSD) (data not shown). These data suggested that BMP ligands are essential for the morphogenesis of OFT, in addition to the septation of aorta and pulmonary artery (Bai et al., 2013; Ma et al., 2005).

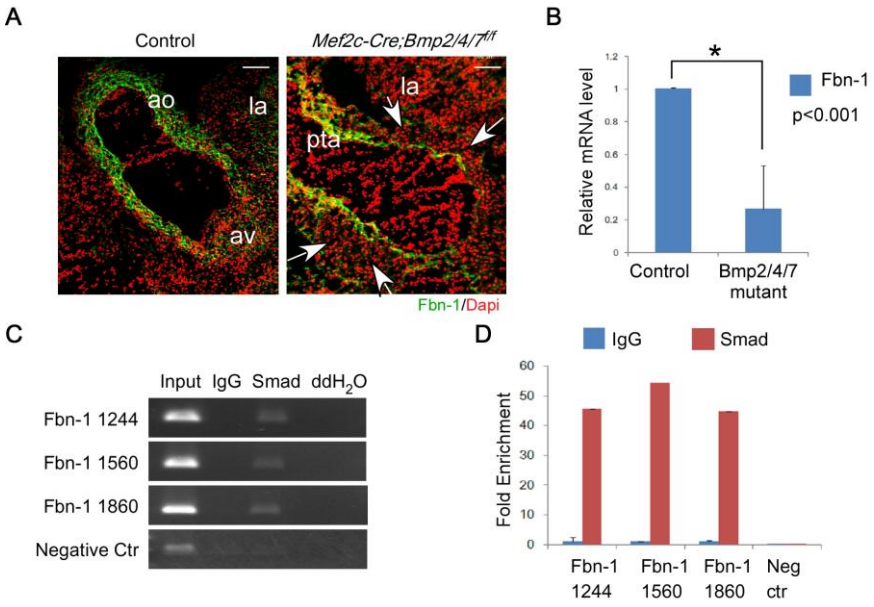

Figure 14. Bmp positively regulate Fbn-1. A: Expression of Fbn1 was examined by immunohisctemistry in the E14.5 hearts of control and Bmp2/4/7 CKO embryos. Arrows in right panel show decrease in Fbn-1 expression. Scale bar (white)=100 μm; la: left atrium; ao: aorta; av: aorta vavle; pta: persistent truncus asteriosus. B: qRT-PCR analysis of aorta tissue of control and Bmp2/4/7 CKO. p-value is analyzed by t-test (two tailed). * P<0.001. (control n=8, mutant n=4). Error bars represent S.E.M. C: ChIP-PCR analysis on Fbn-1 5' upstream regulatory regions. ChIP-PCR on aorta from wild type mice shows the enrichment of flag in regions we interested in. Smad1/5/8 antibody is used to pull down Smad-binding chromatin and after reverse crosslink, DNA is purified to perform PCR. D: Graph shows calculation of fold enrichment of input by ChIP-qPCR. Experiments are run in triplicate. We use ChIP DNA and performed quantitative PCR.

Fbn-1 is positively regulated by BMP signaling

Since Fbn-1 is linked to Marfan syndrome and required for OFT elasticity, we determined the level of Fbn-1 expression in mutant embryos. Fbn-1 expression was dramatically decreased and restricted to the inner layer of OFT root, comparing to the aorta of control embryos (Fig.14A). It was notable that in the area that has fibrillin, the fibrils do not follow the lumen in clear rings in the mutants. qRT-PCR illustrated that mRNA level of Fbn-1 was dramatically decreased in Bmp2/4/7 CKO (Fig. 14B). Surprisingly, we did not detect abnormality of Fbn-1 in the ablation of Bmp4 and Bmp7 (A-7), which suggests that either Bmp2 regulates Fbn-1 expression mainly or the amount of Bmp signal is critical for the maintenance of Fbn-1 during development.

To determine if Fbn-1 transcription is directly regulated by BMP pathway, we analyzed Fbn-1 upstream, and found several putative Smad binding elements (A-8). To validate these binding sites, primers flanking to the sites were designed to detect PCR product on ChIP sample. In the Smad1/5/8 antibody pull-down sample, all three set of primers gave rise to enriched PCR products (Fig. 8C), which suggested direct physical interaction between Smad and chromatin, with 45%, 58%, 42% of fold enrichment correspondingly (Fig. 14D).

Fbn-1 plays a role in Tgf-β sequestration to control bioavailability of the ligands. Thus, we examined the levels of intracellular Tgf-β signaling by determining pSmad2. pSmad2 positive cells was expanded to OFT in Bmp2/4/7 CKO embryos, showing Tgf-β signal pathway was activated by loss of BMP (Fig.15A-D).

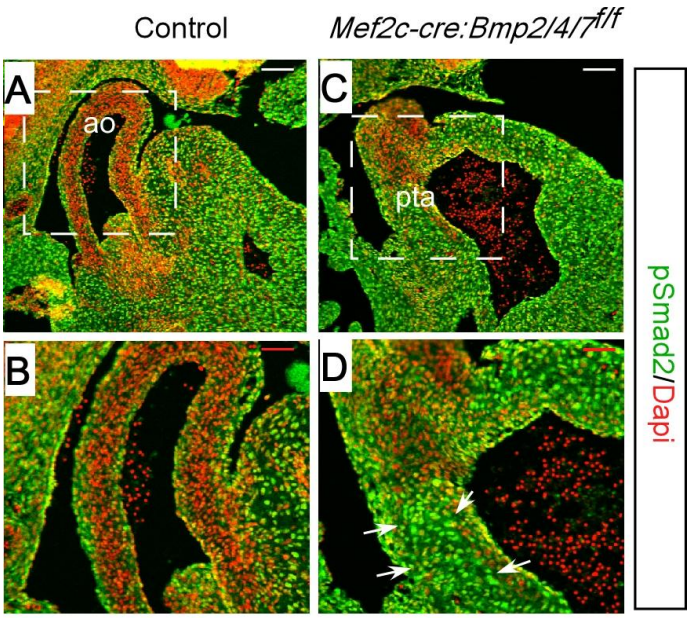

Figure 15. Activation of Tgf-β signal in the absence of Bmp2/4/7. A-D: Immunohistochemical analysis on pSmad2 in the hearts from control (A, B) and Bmp2/4/7 CKO (C, D) at E14.5. Panes B and D are zoomed in images of A and C, respectively. la: left atrium; ra: right atrium; ao: aorta; av: aorta vavle; rv: right ventricle; lv: left ventricle; pta: persistent truncus asteriosus. Scale bar (white)=100 μm; Scale bar (red)=50 μm.

BMP regulates SMC differentiation of the OFT

To further understand the cause of disorganization of the cells in OFT, we examined cell types in the OFT. Majority of the cells in OFT are SMC, however during early development, OFT also expresses cardiac muscle markers around E9.5-E10.5 (Wang et al., 2010). To characterize the OFT cells, we determined the expression of cardiac marker, sarcomeric myosin (MF-20) and smooth muscle marker, alpha-smooth muscle actin (α-SMA) at E14.5. MF-20 was not detected in the control aorta, while it was detected within the mutant OFT. Double staining demonstrated the overlapping expression of MF-20 and α-SMA in CKO OFT (Fig.16A-D).

SHF progenitor marker Isl-1 is reported to control the OFT differentiation at early embryonic stage (Wang et al., 2010), and timely silence of Isl-1 is required for proper development of OFT. To determine if OFT cells in Bmp2/4/7 CKO are progenitor cells, we examined Isl-1 expression. Immunochemistry staining demonstrated that Isl-1 positive cells were persistently existed in BMP mutant, which is not detectable at E14.5 in control (Fig.16E-H). Quantification indicates that Isl-1 positive cells are significant increased in the absence of Bmp2/4/7 (Fig.16I). The results show that the OFT of Bmp2/4/7 CKO embryos is in multi-potent progenitor stage expressing both cardiac and smooth muscle markers, suggesting that BMP regulates SMC differentiation.

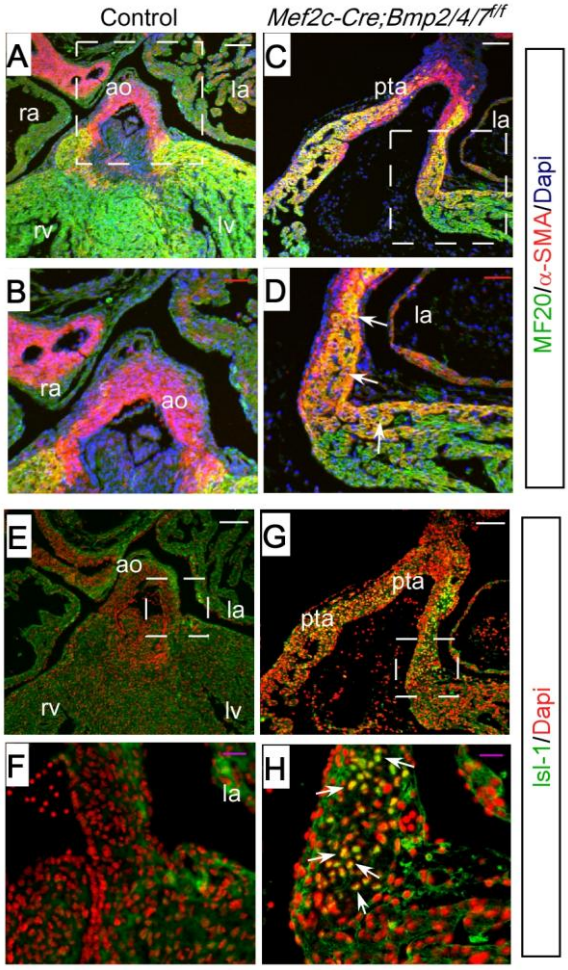

Figure 16. Bmp2/4/7 ablation results in disruption of smooth muscle cell fate. Immunohistochemical analysis is performed on E14.5 hearts of control (A, B, E, F) and Bmp2/4/7 CKO (C, D, G, H). A-D: Immunohistochemical analysis of MF20 (green) and α-SMA (red) on the control (Bmp2/4/7$^{f/f}$) and Bmp2/4/7 CKO OFT. Nuclei are stained with DAPI (blue). Panels B and D are zoomed-in images of B and D, respectively. Arrows in panel D show double staining of MF20 and α-SMA. Scale bar (white)=100 μm; Scale bar (red)=50 μm.E-H: Immunohistochemical analysis on Isl-1 (green). Nuclei are stained with DAPI (red). Panels F and H are zoomed-in images of E and G, respectively. Arrows in panel H shows Isl-1 positive nuclei. la: left atrium; ra: right atrium; ao: aorta; av: aorta vavle; rv: right ventricle; lv: left ventricle; pta: persistent truncus asteriosus. Scale bar (white)=100 μm; Scale bar (purple)=20 μm.

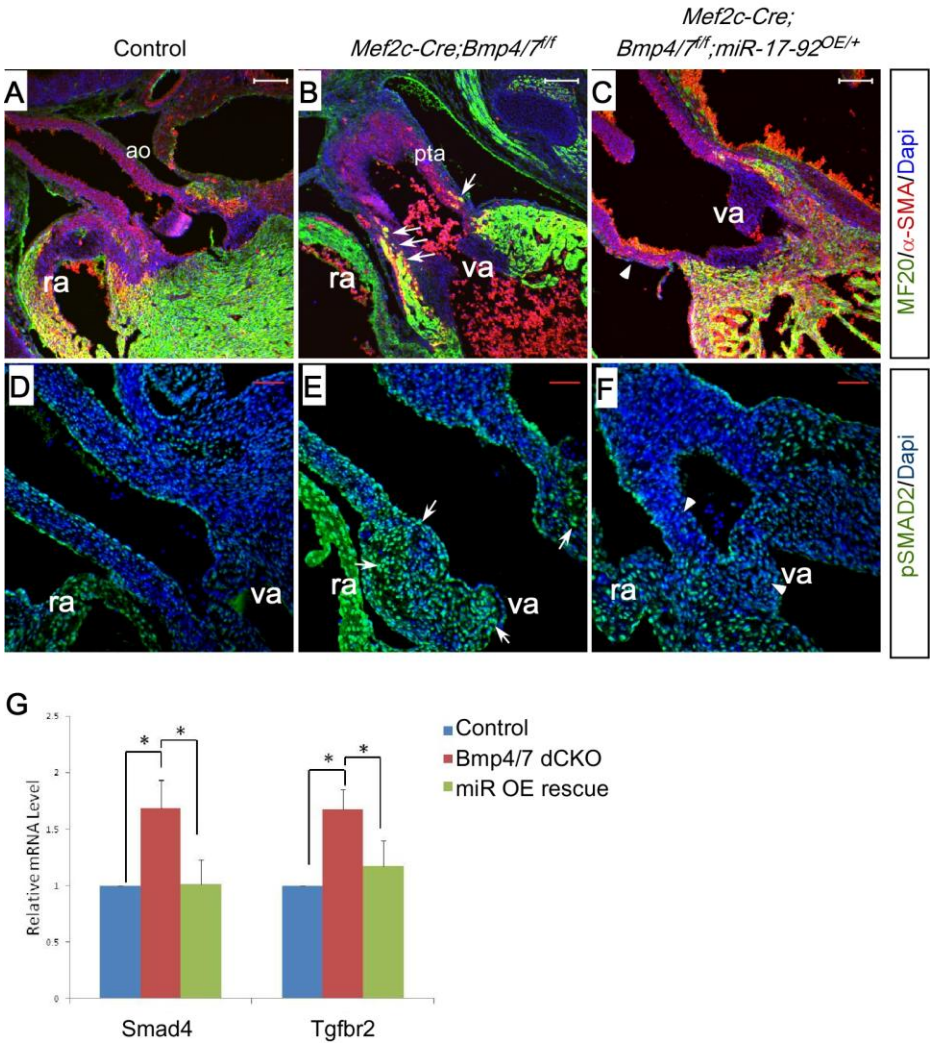

Figure 17. miR-17-92 overexpression partially restores the phenotype. A-F: Immunohistochemical analysis on control (A, D), BMP4/7 CKO (B, E), and BMP4/7 CKO; mir-17-92OE (C, F) hearts from E14.5 embryos. A-C: Immunohistochemical analysis on MF20 and α-SMA on control (Bmp4/7f/f), Bmp4/7 CKO and miR-17-92 OE embyos at E14.5. Arrows in panel B show double positive cells for MF20 and α-SMA expanded in the OFT. and panel C show this expansion is absent in miR-17-92 OE, as shown by arrowhead.) D-F: Immunohistochemical analysis on P-Smad2 on embryos at E14.5. Arrows in panel E show pSmad2 positive cells in OFT and valve; Arrowheads in panel F show the decreased pSmad2 positive cells in OFT and valveScale bar (white)=100 μm. Scale bar (red)=50 μm. G: qRT-PCR of Smad4 and Tgfbr2 in Bmp4/7 mutants, p-value is analyzed by t-test (two tailed). * $P<0.05$. (control n=4, Bmp4/7 dCKO n=4, miR OE n=4). Error bars represent S.E.M.

MiR-17-92 overexpression can suppress the OFT defects in BMP mutants

miR-17-92 is a downstream target of BMP pathway and its overexpression can partial rescue loss of BMP signaling in myocardium development and OFT septation (Bai et al., 2013; Wang et al., 2010). Thus, we determined if overexpression of miR-17-92 can rescue the aortic aneurysm caused by loss of BMP in OFT. Here we used Bmp4/7 dCKO (*Mef2c-Cre;Bmp4/7*$^{f/f}$) instead of Bmp2/4/7 CKO since Bmp4/7 CKO show similar phenotype to that of Bmp2/4/7.

Bmp4/7 dCKO showed thickening and disorganized OFT similar to Bmp2/4/7 CKO (A-6). Overexpressinon of miR-17-92 in Bmp4/7 dCKO background (*Mef2c-Cre;Bmp4/7*^{f}*/f;miR-17-92*$^{OE/+}$) exhibited the truncus with normal width and cell morphology (A-6), indicating the defects of OFT in Bmp4/7 CKO was rescued by miR-17-92 overexpression. To determine if SMC differentiation is rescued, we performed immunostaining of MF20 and α-SMA. Expression pattern of MF20 and α-SMA in miR-17-92 OE was comparable to control, showing that overexpressing miR-17-92 does not alter SMC differentition. Expression of both MF-20 and α-SMA were detected in OFT of *Mef2c-Cre;Bmp4/7*^{f}*/*^{f}*;miR-17-92*$^{OE/+}$, but expansion of MF-20 is rescued compare to Bmp2/4/7 CKO (Fig.17A-C), indicating SMC differentiation is partially rescued by miR-17-92. Level of pSmad2 was decreased compare to Bmp4/7 dCKO by miR-17-92 overexpression in BMP4/7 background (Fig.17D-F). Smad4 and Tgfbr2 mRNA levels are significant restored by overexpression of miR-17-92 compared to Bmp4/7 dCKO (Fig.17G). In addition, overexpression of miR-17-92 repressed Isl-1 expression to some extent in BMP4/7 background (A-9, D-F, G-I). All these data indicate that

overexpression of miR-17-92 can rescue the defects in cell determination and maintaining its cell fate caused by absence of BMP signals.

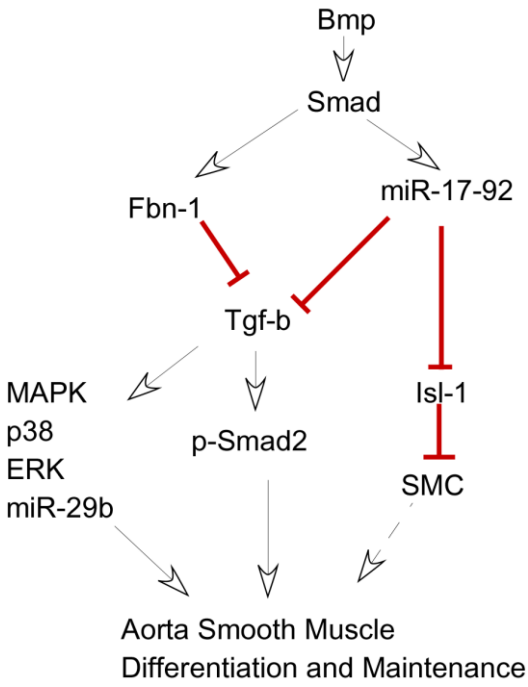

Figure 18. Working model of Bmp regulation in Aorta aneurysm. Bmp regulate expression of Fbn-1 and SMC differentiation through Smad. Fbn-1 controls Tgf-β signal in normal condition. miR-17-92 plays important roles in control Tgf-b signal and Isl-1 silencing. In addition, non-canonical Tgf-b signal pathway, such as MAPK, p38, ERK, mir-29b are also involved in the contribution of aorta aneurysm based on recent studies.

Discussion

In this manuscript, we showed that BMP signals is involved in aortic aneurysm during development and in the adult. BMP pathway regulates expression of Fbn-1 directly through Smad and suppress Tgf-β signaling. BMP pathway also directs SMC differentiation in the aorta. Furthermore, we showed that miR-17-92 can partially rescue loss of BMP for SMC differentiation and suppression of Tgf-β signaling. Taken together, we propose the model of BMP regulation in Fig. 18.

Homostasis of TGF-β signal and MFS

Examination of plasma sample show that circulating total Tgf-β1 concentrations are significant increased in MFS patients without cardiovascular drug treatment compared to control individual, while MFS patients treated with losartan or β-blocker show dramatically lower Tgf-β1 concentration compared with untreated patients (Matt et al., 2009). Mutation in Tgf-β is identified in some of Marfan patients (Neptune et al., 2003). Although the majority mutation of Tgf-β are indicated to affect the proper function of these proteins, diseased aortic tissue from Marfan Syndrome patients show increased p-Smad2 in aortic SMCs (Attias et al., 2009; Boileau et al., 2012; Loeys et al., 2006), consist with the phenotype we found in BMP mouse model. Surprisingly, decreased Tgf-β signal also exacerbates aorta aneurysm in mouse model. Recent study onTgfbr2 inactivation in postnatal SMCs shows rapid aorta thickening, dilation and dissection (Li et al., 2014).it suggests that basal TGF-β signal is important to maintain aortic wall homeostasis and normal function of aortic smooth muscle. MAPK and p38

signal pathway are reported to contribute to aorta malfunction in Tgf-β disrupted mouse model.

Unlike Tgf-β, BMP has not been reported to be genetically associated with Marfan syndrome although it is a member of Tgf-β superfamily. However, regulation of BMP and Tgf-β bioactivity by Fbn-1 is proposed in bone formation. There are possible several reasons why the role of BMP in Marfan syndrome is poor studied. First, BMP ligands are functional redundant that single mutation is not enough to exhibit phenotype. Second, compound mutations result in embryonic lethal that make it impossible to study afterbirth phenotype. Bmp2/4/7 triple CKO die around E16.5-E18.5. Bmp4/7 and Bmp2/4 dCKO is also embryonic lethal (Bai et al., 2013; Wang et al., 2010). Third, early perturbations might result in later-onset phenotype in adulthood, but it's hard to trace back. In our study, we found that Bmp4;Fbn-1 dHet developed severer aorta aneurysm than *Fbn-1*$^{C1039G/+}$ by itself. Although Bmp4 heterozygous is viable due to compensation of other BMPligands, the gross morphology of aorta is abnormal comparing to its littermates. Haploinsufficent of Bmp4 makes the adult mice predisposed to severe aneurysm. It is possible that in aorta aneurysm patients, some of this population might have disturbed BMP signals during the embryonic stage. Activation of Tgf-β signals also bring up a possibility that maybe Losartan treatment can help the phenotype observed in BMP mutant. Further experiments are needed to address this hypothesis.

BMP-YAP signal pathway to regulate SMC homeostasis

Previous studies show that Yap can form complex with linker-phosphorylated Smad (Alarcon et al., 2009). Phosphorylated Yap is located in cytoplasm indicated the

activation of Hippo pathway (Heallen et al., 2013; Heallen et al., 2011). In our preliminary data (not shown), we found that nucleus Yap is significant increased on stiffer matrix compared to soft matrix, which suggest that Yap and Smad can regulate genes that are important for SMC homeostasis in the context of high mechanical stress matrix. In the MFS patient, aorta stiffness is increased, SMC is fragmented and aorta is easier to rupture. In our Bmp mutant mouse model, the deletion of Bmps results in the downregulation of nucleus Smad1/5/8 in Smooth Muscle cells, which in turn will not be sufficient to form complex with Yap to regulate their downstream genes in the context of stiffer SMC. However, it is still not clear if it is a cause or effect. Besides, the balance between activation of pSmad2 and inactivation of Smad1/5/8 is still not well understood with regard to the cooperative effect with Yap. More researches are needed to be done to test this hypothesis. Moreover, it is also interesting to explore if Fbn is moderated by Smad-Yap complex.

MicroRNA-mediated SMC differentiation by BMP and MFS

Studies in MFS illustrated genes involved in comtractile SMCs are responsible for aortic diseases. MYH11, ACTA2 mutations in human result in aortic aneurysm and dissection due to perturbed contractile apparatus (Milewicz et al., 2008). Interestingly, SMCs are not terminally differentiated even in adult. They retain phenotypic plasticity and can de-differentiated in response to vascular injury or environmental cues including growth factors/inhibitors, mechanical influences and ect.

In our previous study, we found that miR participated in OFT smooth muscle differentiation (Wang et al., 2010). However, not so many microRNAs are found to be

involved in Marfan syndrome. Increased miR-29b is detected in early aneurysm development of MFS by regulating aortic wall apoptosis and extracelluar matrix abnormalities. In our study, we found that miR-17-92 can partially restore Bmp4/7 dCKO phenotype. However, due to the Cre activity and limited increased fold of miR, it is still not clear to what extent and at what amount that miR-17-92 can help with Marfan syndrome. Interestingly, we also find a miR-17-92 binding site in 3'UTR of Fbn-1, which means Fbn-1 is a potential target of miR-17-92, the feed back loop makes the rescue event even more complicated. The other question we are trying to address here is that whether activation of Isl-1, a downstream target of miR-17-92, is the cause or the effect in our mouse model. There are two possibilities, 1) lack of inhibition-the cause. BMP positively regulate miR-17-92 transcription which is responsible for the inhibition of Isl-1 at certain time window. Deficiency of BMP results in decreased miR-17-92 and later activation of Isl-1 expression which results in the multi-potent cell state of "smooth muscle cells", along with the gross morphology change; 2) lack of differentiation-the effect. Ectopic expression of MF20 contributes to the de-differentiation of smooth muscle cells, and this de-differentiation triggers smooth muscle cell repair system to activate Isl-1 expression. In the miR-17-92 overexpression mouse model, we found that Isl-1 is decreased and ectopic MF20 expression is diminished. It indicates that MF20 is inhibited by miR-17-92 by suppression of Isl-1, in other words, activated Isl-1 facilitates MF20 expression. Although we did not detect difference of α-SMA protein expression in either mutants, but can't rule out any subtle change of cell structure and architecture, considering the extreme morphology change in Bmp2/4/7 CKO. These data suggest that

therapeutic manipulation of miR-17-92 and its target genes holds promise for ameliorate TAA disease progression and protecting from dissection.

BMP deficiency, hypoxia and inflammation in aorta aneurysm

Great vessels are maintained by blood perfushion in the lumen as well as Vasa Vasorum (VV) through unclear mechanism. VV is especially important for the normal function of adventitia and media of great vessels. Hypoxia induces abnormality of VV, including the hyperplasia of smooth muscle, and enlargement and expansion of VV. In our mouse model, we found that smooth muscle, which called media when developed, of BMP mutants are impressively messed up, with very fat and loosen morphology and increased VV in the adventitia layer (data not shown). Intriguingly, BMP mutants have VSD and valve defect, which might be the cause of hypoxia of vessels. Therefore, whether the disturbance of VV is the cause of weaken smooth muscle layer or the result of VSD phenotype is still need to be addressed in the future work. Weakened smooth muscle is responsible for the rupture of aorta aneurysm. The concept that hypoxia can cause inflammation has gained widely acceptance. Most aneurysm patients have upregulated proteolytic pathways within the medial layer of the arterial wall. MMP2 and MMP9 activities are increased in aneurysm formation, as well as HIF-1α, which is considered to accelerate MMP production from macrophages (Tanaka et al., 2013). It is believed that the abnormal processing of Fbn-1 by SMCs can trigger the detachment of vascular SMCs from extracellular matrix, which result in the MMP upregulation. Therefore, the matrix disruption and elastin fragmentation cause SMCs apoptosis and abnormality of the media layer, which worsen the aorta structure (Fedak et al., 2003).

Summary

Marfan syndrome (MFS) is a disease which occurs 1 in 5000 people, and its patients have complex symptoms found in the heart, blood vessels, bones and eyes. Aortic aneurysm of Marfan syndrome patients is the most risk that results in sudden death and mutation in *Fibrillin-1* (*Fbn-1*) has been linked to its cause. However, mutation in other genes has been associated with Marfan syndrome. Here, we determined that the roles of BMP signaling in aortic aneurysm. Since knockout animals of BMP ligands do not survive till adulthood, we analyzed $Fbn^{C1039G/+}$; *Mef2c-Cre;*$Bmp4^{f/+}$ double heterozygous mice to investigate the interaction between Fbn-1 and BMP signal pathway. Adult mice heterozygous for both *Bmp4* and *Fbn-1* developed dilated aorta root earlier than $Fbn^{C1039G/+}$, which indicates that decreased level of *Bmp4* aggravates aorta aneurysm in *Fbn* mutant background. To further characterize the roles of BMP in OFT development, we analyzed the embryos lacking BMP ligands. *Bmp2/4/7* triple CKO (*Mef2c-Cre;Bmp2/4/7*$^{f/f}$) exhibit disorganization in tuncus during development. Both *Fbn-1* mRNA and its protein level are decreased in the absence of *Bmp2/4/7*. Bioinformatic analysis and ChIP-PCR suggest that Smad binds to *Fbn-1* chromatin, indicating that Fbn-1 is directly regulated by BMP signal. Similar to *Fbn-1* mutant, pSmad2 is activated in the OFT of *Bmp2/4/7* CKO, further supporting that BMP signal is upstream of Fbn-1. Characterization of the cells in mutant truncus revealed that they are multi-potent cells expressing both sarcomeric myosin and α-smooth muscle actin and expressing Isl-1, the cardiac progenitor factor. Our study suggests that BMP

signal is involved in Marfan syndrome by regulating aorta smooth muscle differentiation and modifying the pathway can treat the disease.

CHAPTER IV

CONCLUSION

Studies on Bmp during development stage reveal that Bmps are not only the major player for dorsal-ventral axis specification, but also important for organ formation and differentiation. Our studies on developing heart suggest that Bmps are critical for cardiogenesis. Disturbance of Bmp signals results in the malformation of heart tube and subsequent heart diseases. One of the steps in heart development is EMT, which is the pivotal step that controlled by Bmp signals during specific region and certain development stage, spatially and temporally**.** Our studies show defect of EMT in Bmp mutant eventually causes septum defect, valve abnormality and AP separation. *Vegfa* as a downstream target of Bmp signal pathway is tightly controlled by Smad- and miR-dependent mechanism (Fig. 19). Suppression of *Vegfa* is required for the non-invasive EMT of OFT at E10.5, Twist1/2, snail, slug and Id1/2 are important for the invasive EMT. Disruption of the EMT process will result in the absence of cushion mesenchyme in the OFT and subsequent defect.

Haploinsufficiency of Bmp4 does not show obvious developmental defect, but this small change in embryonic stage makes adult mice more predisposed to aorta dilation and rupture, which indicates the early onset of heart disease due to the minor disturbance occurred on embryogenesis. Our studies showed that Bmp2, -4, -7 are critical for EMT process and smooth muscle differentiation and maintenance during development, which may be important for the mechanic stress sense of the great vessels of heart. Inhibition of Isl-1 by miR-17-92 is essential for the proper differentiation of

smooth muscle cells. Activation of pSmad2 by either canonical or noncanonical Tgf-β signal pathway contribute to the aorta aneurysm (Fig. 19). Disturbance of Bmp signals makes the mice susceptible to aorta dialation.

We showed that miRNAs are involved in some of the BMP pathways. miRNAs has been and will be a direction for treatment of congenital heart disease. To explore mechanism behinds miRNAs and signal pathway network, more examination is needed to test the effect of miRNA on signal pathway as well as the side effects. However, it still sheds a light on the new therapy on congenital heart disease, and it will be more interesting to understand if the correction of signal pathway activity in adult stage can rescue the phenotype caused by embryonic stage.

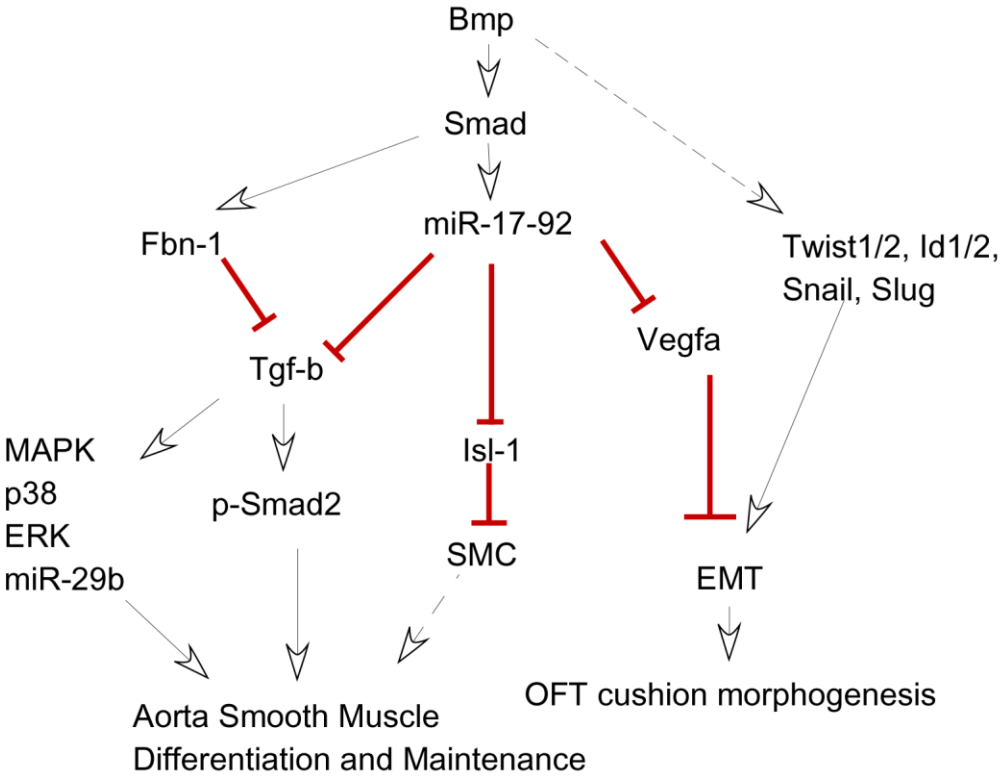

Figure 19. Working model of Bmp regulation in OFT and aorta maintenance. Bmp signals regulate its target gens by Smad- or mR-dependent mechanism.

REFERENCES

Alarcon, C., Zaromytidou, A.I., Xi, Q., Gao, S., Yu, J., Fujisawa, S., Barlas, A., Miller, A.N., Manova-Todorova, K., Macias, M.J., *et al.* (2009). Nuclear CDKs drive Smad transcriptional activation and turnover in BMP and TGF-beta pathways. Cell *139*, 757-769.

Arteaga-Solis, E., Gayraud, B., Lee, S.Y., Shum, L., Sakai, L., and Ramirez, F. (2001). Regulation of limb patterning by extracellular microfibrils. The Journal of Cell Biology *154*, 275-282.

Attias, D., Stheneur, C., Roy, C., Collod-Béroud, G., Detaint, D., Faivre, L., Delrue, M.-A., Cohen, L., Francannet, C., Béroud, C., *et al.* (2009). Comparison of Clinical Presentations and Outcomes Between Patients With TGFBR2 and FBN1 Mutations in Marfan Syndrome and Related Disorders. Circulation *120*, 2541-2549.

Bai, Y., Wang, J., Morikawa, Y., Bonilla-Claudio, M., Klysik, E., and Martin, J.F. (2013). Bmp signaling represses Vegfa to promote outflow tract cushion development. Development *140*, 3395-3402.

Boileau, C., Guo, D.-C., Hanna, N., Regalado, E.S., Detaint, D., Gong, L., Varret, M., Prakash, S.K., Li, A.H., d'Indy, H., *et al.* (2012). TGFB2 mutations cause familial thoracic aortic aneurysms and dissections associated with mild systemic features of Marfan syndrome. Nat Genet *44*, 916-921.

Bonilla-Claudio, M., Wang, J., Bai, Y., Klysik, E., Selever, J., and Martin, J.F. (2012). Bmp signaling regulates a dose-dependent transcriptional program to control facial skeletal development. Development *139*, 709-719.

Brand, T. (2003). Heart development: molecular insights into cardiac specification and early morphogenesis. Developmental Biology *258*, 1-19.

Bressan, M., Liu, G., and Mikawa, T. (2013). Early Mesodermal Cues Assign Avian Cardiac Pacemaker Fate Potential in a Tertiary Heart Field. Science *340*, 744-748.

Bruneau, B.G. (2008). The developmental genetics of congenital heart disease. Nature *451*, 943-948.

Cascio, S., D'Andrea, A., Ferla, R., Surmacz, E., Gulotta, E., Amodeo, V., Bazan, V., Gebbia, N., and Russo, A. (2010). miR-20b modulates VEGF expression by targeting HIF-1α and STAT3 in MCF-7 breast cancer cells. Journal of Cellular Physiology *224*, 242-249.

Chan, M.C., Weisman, A.S., Kang, H., Nguyen, P.H., Hickman, T., Mecker, S.V., Hill, N.S., Lagna, G., and Hata, A. (2011). The Amiloride Derivative Phenamil Attenuates Pulmonary Vascular Remodeling by Activating NFAT and the Bone Morphogenetic Protein Signaling Pathway. Molecular and Cellular Biology *31*, 517-530.

Chang, C.-P., Neilson, J.R., Bayle, J.H., Gestwicki, J.E., Kuo, A., Stankunas, K., Graef, I.A., and Crabtree, G.R. (2004). A Field of Myocardial-Endocardial NFAT Signaling Underlies Heart Valve Morphogenesis. Cell *118*, 649-663.

Choudhary, B., Zhou, J., Li, P., Thomas, S., Kaartinen, V., and Sucov, H.M. (2009). Absence of TGFβ signaling in embryonic vascular smooth muscle leads to reduced lysyl oxidase expression, impaired elastogenesis, and aneurysm. genesis *47*, 115-121.

Damert, A., Miquerol, L., Gertsenstein, M., Risau, W., and Nagy, A. (2002). Insufficient VEGFA activity in yolk sac endoderm compromises haematopoietic and endothelial differentiation. Development *129*, 1881-1892.

Davis, B.N., Hilyard, A.C., Lagna, G., and Hata, A. (2008). SMAD proteins control DROSHA-mediated microRNA maturation. Nature *454*, 56-61.

Dȯot, E.C., Bahamonde, M.E., Zhao, M., and Lyons, K.M. (2003). BMP signaling is required for septation of the outflow tract of the mammalian heart. Development *130*, 209-220.

Dietz, H., and Pyeritz, R. (1995). Mutations in the human gene for fibrillin-1 (FBN1) in the Marfan syndrome and related disorders. Human Molecular Genetics *4*, 1799-1809.

Dietz, H.C., Cutting, C.R., Pyeritz, R.E., Maslen, C.L., Sakai, L.Y., Corson, G.M., Puffenberger, E.G., Hamosh, A., Nanthakumar, E.J., Curristin, S.M., *et al.* (1991). Marfan syndrome caused by a recurrent de novo missense mutation in the fibrillin gene. Nature *352*, 337-339.

Dudley, A.T., and Robertson, E.J. (1997). Overlapping expression domains of bone morphogenetic protein family members potentially account for limited tissue defects in BMP7 deficient embryos. Developmental Dynamics *208*, 349-362.

Fedak, P.W., de Sa, M.P., Verma, S., Nili, N., Kazemian, P., Butany, J., Strauss, B.H., Weisel, R.D., and David, T.E. (2003). Vascular matrix remodeling in patients with

bicuspid aortic valve malformations: implications for aortic dilatation. J Thorac Cardiovasc Surg *126*, 797-806.

Ferrara, N., Carver-Moore, K., Chen, H., Dowd, M., Lu, L., O'Shea, K.S., Powell-Braxton, L., Hillan, K.J., and Moore, M.W. (1996). Heterozygous embryonic lethality induced by targeted inactivation of the VEGF gene. Nature *380*, 439-442.

Furuta, Y., Piston, D.W., and Hogan, B.L. (1997). Bone morphogenetic proteins (BMPs) as regulators of dorsal forebrain development. Development *124*, 2203-2212.

Groenink, M., den Hartog, A.W., Franken, R., Radonic, T., de Waard, V., Timmermans, J., Scholte, A.J., van den Berg, M.P., Spijkerboer, A.M., Marquering, H.A., *et al.* (2013). Losartan reduces aortic dilatation rate in adults with Marfan syndrome: a randomized controlled trial. European Heart Journal *34*, 3491-3500.

Haigh, J.J., Gerber, H.P., Ferrara, N., and Wagner, E.F. (2000). Conditional inactivation of VEGF-A in areas of collagen2a1 expression results in embryonic lethality in the heterozygous state. Development *127*, 1445-1453.

Harvey, R.P. (2002). Patterning the vertebrate heart. Nat Rev Genet *3*, 544-556.

Heallen, T., Morikawa, Y., Leach, J., Tao, G., Willerson, J.T., Johnson, R.L., and Martin, J.F. (2013). Hippo signaling impedes adult heart regeneration. Development *140*, 4683-4690.

Heallen, T., Zhang, M., Wang, J., Bonilla-Claudio, M., Klysik, E., Johnson, R.L., and Martin, J.F. (2011). Hippo pathway inhibits Wnt signaling to restrain cardiomyocyte proliferation and heart size. Science *332*, 458-461.

Henningfeld, K.A., Rastegar, S., Adler, G., and Knöchel, W. (2000). Smad1 and Smad4 Are Components of the Bone Morphogenetic Protein-4 (BMP-4)-induced Transcription Complex of the Xvent-2B Promoter. Journal of Biological Chemistry *275*, 21827-21835.

Hogan, B.L.M. (1996). Bone morphogenetic proteins in development. Current Opinion in Genetics & Development *6*, 432-438.

Holm, T.M., Habashi, J.P., Doyle, J.J., Bedja, D., Chen, Y., van Erp, C., Lindsay, M.E., Kim, D., Schoenhoff, F., Cohn, R.D., *et al.* (2011). Noncanonical TGFβ Signaling Contributes to Aortic Aneurysm Progression in Marfan Syndrome Mice. Science *332*, 358-361.

Inamoto, S., Kwartler, C.S., Lafont, A.L., Liang, Y.Y., Fadulu, V.T., Duraisamy, S., Willing, M., Estrera, A., Safi, H., Hannibal, M.C., *et al.* (2010). TGFBR2 mutations alter smooth muscle cell phenotype and predispose to thoracic aortic aneurysms and dissections. Cardiovascular Research *88*, 520-529.

Ishida, W., Hamamoto, T., Kusanagi, K., Yagi, K., Kawabata, M., Takehara, K., Sampath, T.K., Kato, M., and Miyazono, K. (2000). Smad6 Is a Smad1/5-induced Smad Inhibitor. Journal of Biological Chemistry *275*, 6075-6079.

Itoh, S., Itoh, F., Goumans, M.-J., and ten Dijke, P. (2000). Signaling of transforming growth factor-β family members through Smad proteins. European Journal of Biochemistry *267*, 6954-6967.

Jain, D., Dietz, H.C., Oswald, G.L., Maleszewski, J.J., and Halushka, M.K. (2011). Causes and histopathology of ascending aortic disease in children and young adults. Cardiovascular Pathology *20*, 15-25.

Jones, C.M., Lyons, K.M., and Hogan, B.L. (1991). Involvement of Bone Morphogenetic Protein-4 (BMP-4) and Vgr-1 in morphogenesis and neurogenesis in the mouse. Development *111*, 531-542.

Judge, D.P., Biery, N.J., Keene, D.R., Geubtner, J., Myers, L., Huso, D.L., Sakai, L.Y., and Dietz, H.C. (2004). Evidence for a critical contribution of haploinsufficiency in the complex pathogenesis of Marfan syndrome. The Journal of Clinical Investigation *114*, 172-181.

Kaartinen, V., Dudas, M., Nagy, A., Sridurongrit, S., Lu, M.M., and Epstein, J.A. (2004). Cardiac outflow tract defects in mice lacking ALK2 in neural crest cells. Development *131*, 3481-3490.

Karaulanov, E., Knochel, W., and Niehrs, C. (2004). Transcriptional regulation of BMP4 synexpression in transgenic Xenopus. EMBO J *23*, 844-856.

Kawabata, M., Imamura, T., and Miyazono, K. (1998). Signal transduction by bone morphogenetic proteins. Cytokine & Growth Factor Reviews *9*, 49-61.

Khalil, N. (1999). TGF-β: from latent to active. Microbes and Infection *1*, 1255-1263.

Koralov, S.B., Muljo, S.A., Galler, G.R., Krek, A., Chakraborty, T., Kanellopoulou, C., Jensen, K., Cobb, B.S., Merkenschlager, M., Rajewsky, N., *et al.* (2008). Dicer Ablation Affects Antibody Diversity and Cell Survival in the B Lymphocyte Lineage. Cell *132*, 860-874.

Korchynskyi, O., and ten Dijke, P. (2002). Identification and functional characterization of distinct critically important bone morphogenetic protein-specific response elements in the Id1 promoter. J Biol Chem *277*, 4883-4891.

Koshiba-Takeuchi, K., Mori, A.D., Kaynak, B.L., Cebra-Thomas, J., Sukonnik, T., Georges, R.O., Latham, S., Beck, L., Henkelman, R.M., Black, B.L., *et al.* (2009). Reptilian heart development and the molecular basis of cardiac chamber evolution. Nature *461*, 95-98.

Lawson, K.A., Dunn, N.R., Roelen, B.A.J., Zeinstra, L.M., Davis, A.M., Wright, C.V.E., Korving, J.P.W.F.M., and Hogan, B.L.M. (1999). Bmp4 is required for the generation of primordial germ cells in the mouse embryo. Genes & Development *13*, 424-436.

Li, W., Li, Q., Jiao, Y., Qin, L., Ali, R., Zhou, J., Ferruzzi, J., Kim, R.W., Geirsson, A., Dietz, H.C., *et al.* (2014). Tgfbr2 disruption in postnatal smooth muscle impairs aortic wall homeostasis. The Journal of Clinical Investigation *124*, 0-0.

Liu, W., Selever, J., Wang, D., Lu, M.-F., Moses, K.A., Schwartz, R.J., and Martin, J.F. (2004). Bmp4 signaling is required for outflow-tract septation and branchial-arch artery remodeling. Proceedings of the National Academy of Sciences of the United States of America *101*, 4489-4494.

Loeys, B.L., Schwarze, U., Holm, T., Callewaert, B.L., Thomas, G.H., Pannu, H., De Backer, J.F., Oswald, G.L., Symoens, S., Manouvrier, S., *et al.* (2006). Aneurysm Syndromes Caused by Mutations in the TGF-β Receptor. New England Journal of Medicine *355*, 788-798.

Long, J., Wang, Y., Wang, W., Chang, B.H.J., and Danesh, F.R. (2010). Identification of MicroRNA-93 as a Novel Regulator of Vascular Endothelial Growth Factor in Hyperglycemic Conditions. Journal of Biological Chemistry *285*, 23457-23465.

Lu, M.-F., Pressman, C., Dyer, R., Johnson, R.L., and Martin, J.F. (1999). Function of Rieger syndrome gene in left-right asymmetry and craniofacial development. Nature *401*, 276-278.

Luna-Zurita, L., Prados, B., Grego-Bessa, J., Luxán, G., del Monte, G., Benguría, A., Adams, R.H., Pérez-Pomares, J.M., and de la Pompa, J.L. (2010). Integration of a Notch-dependent mesenchymal gene program and Bmp2-driven cell invasiveness regulates murine cardiac valve formation. The Journal of Clinical Investigation *120*, 3493-3507.

Ma, L., Lu, M.-F., Schwartz, R.J., and Martin, J.F. (2005). Bmp2 is essential for cardiac cushion epithelial-mesenchymal transition and myocardial patterning. Development *132*, 5601-5611.

Maegdefessel, L., Azuma, J., Toh, R., Merk, D.R., Deng, A., Chin, J.T., Raaz, U., Schoelmerich, A.M., Raiesdana, A., Leeper, N.J., *et al.* (2012). Inhibition of microRNA-29b reduces murine abdominal aortic aneurysm development. The Journal of Clinical Investigation *122*, 497-506.

Matt, P., Schoenhoff, F., Habashi, J., Holm, T., Van Erp, C., Loch, D., Carlson, O.D., Griswold, B.F., Fu, Q., De Backer, J., *et al.* (2009). Circulating Transforming Growth Factor-β in Marfan Syndrome. Circulation *120*, 526-532.

McCulley, D.J., Kang, J.-O., Martin, J.F., and Black, B.L. (2008). BMP4 is required in the anterior heart field and its derivatives for endocardial cushion remodeling, outflow tract septation, and semilunar valve development. Developmental Dynamics *237*, 3200-3209.

Milewicz, D.M., Guo, D.-C., Tran-Fadulu, V., Lafont, A.L., Papke, C.L., Inamoto, S., Kwartler, C.S., and Pannu, H. (2008). Genetic Basis of Thoracic Aortic Aneurysms and Dissections: Focus on Smooth Muscle Cell Contractile Dysfunction. Annual Review of Genomics and Human Genetics *9*, 283-302.

Mirick, A.L., Patel, H.J., Deeb, G.M., and Williams, D.M. (2013). Aortic Intussusception Complicating Diagnostic Angiography: Recognition and Management. The Annals of Thoracic Surgery *95*, 1776-1778.

Miyazono, K., Kamiya, Y., and Morikawa, M. (2010). Bone morphogenetic protein receptors and signal transduction. Journal of Biochemistry *147*, 35-51.

Nakashima, M., and Reddi, A.H. (2003). The application of bone morphogenetic proteins to dental tissue engineering. Nat Biotech *21*, 1025-1032.

Neptune, E.R., Frischmeyer, P.A., Arking, D.E., Myers, L., Bunton, T.E., Gayraud, B., Ramirez, F., Sakai, L.Y., and Dietz, H.C. (2003). Dysregulation of TGF-[beta] activation contributes to pathogenesis in Marfan syndrome. Nat Genet *33*, 407-411.

Nistala, H., Lee-Arteaga, S., Smaldone, S., Siciliano, G., Carta, L., Ono, R.N., Sengle, G., Arteaga-Solis, E., Levasseur, R., Ducy, P., *et al.* (2010). Fibrillin-1 and -2 differentially modulate endogenous TGF-β and BMP bioavailability during bone formation. The Journal of Cell Biology *190*, 1107-1121.

Olson, E.N. (2006). Gene Regulatory Networks in the Evolution and Development of the Heart. Science *313*, 1922-1927.

Reddi, A.H. (1998). Role of morphogenetic proteins in skeletal tissue engineering and regeneration. Nat Biotech *16*, 247-252.

Selever, J., Liu, W., Lu, M.-F., Behringer, R.R., and Martin, J.F. (2004). Bmp4 in limb bud mesoderm regulates digit pattern by controlling AER development. Developmental Biology *276*, 268-279.

Shi, Y. (1998). Crystal structure of a Smad MH1 domain bound to DNA: insights on DNA-binding in TGF[bgr] signaling. Cell *94*, 585-594.

Shi, Y., and Massagué, J. (2003). Mechanisms of TGF-β Signaling from Cell Membrane to the Nucleus. Cell *113*, 685-700.

Solloway, M.J., and Robertson, E.J. (1999). Early embryonic lethality in Bmp5;Bmp7 double mutant mice suggests functional redundancy within the 60A subgroup. Development *126*, 1753-1768.

Stankunas, K., Ma, G.K., Kuhnert, F.J., Kuo, C.J., and Chang, C.-P. (2010). VEGF signaling has distinct spatiotemporal roles during heart valve development. Developmental Biology *347*, 325-336.

Stottmann, R.W., Choi, M., Mishina, Y., Meyers, E.N., and Klingensmith, J. (2004). BMP receptor IA is required in mammalian neural crest cells for development of the cardiac outflow tract and ventricular myocardium. Development *131*, 2205-2218.

Tanaka, H., Zaima, N., Sasaki, T., Hayasaka, T., Goto-Inoue, N., Onoue, K., Ikegami, K., Morita, Y., Yamamoto, N., Mano, Y., *et al.* (2013). Adventitial Vasa Vasorum Arteriosclerosis in Abdominal Aortic Aneurysm. PLoS ONE *8*, e57398.

Tomita, M., Reinhold, M.I., Molkentin, J.D., and Naski, M.C. (2002). Calcineurin and NFAT4 Induce Chondrogenesis. Journal of Biological Chemistry *277*, 42214-42218.

van Rooij, E., Sutherland, L.B., Thatcher, J.E., DiMaio, J.M., Naseem, R.H., Marshall, W.S., Hill, J.A., and Olson, E.N. (2008). Dysregulation of microRNAs after myocardial infarction reveals a role of miR-29 in cardiac fibrosis. Proceedings of the National Academy of Sciences *105*, 13027-13032.

Ventura, A., Young, A.G., Winslow, M.M., Lintault, L., Meissner, A., Erkeland, S.J., Newman, J., Bronson, R.T., Crowley, D., Stone, J.R., *et al.* (2008). Targeted Deletion Reveals Essential and Overlapping Functions of the miR-17~92 Family of miRNA Clusters. Cell *132*, 875-886.

Verzi, M.P., McCulley, D.J., De Val, S., Dodou, E., and Black, B.L. (2005). The right ventricle, outflow tract, and ventricular septum comprise a restricted expression domain within the secondary/anterior heart field. Developmental Biology *287*, 134-145.

Vincentz, J.W., Barnes, R.M., Rodgers, R., Firulli, B.A., Conway, S.J., and Firulli, A.B. (2008). An absence of Twist1 results in aberrant cardiac neural crest morphogenesis. Developmental Biology *320*, 131-139.

Wang, J., Bai, Y., Li, H., Greene, S.B., Klysik, E., Yu, W., Schwartz, R.J., Williams, T.J., and Martin, J.F. (2013). MicroRNA-17-92, a direct Ap-2alpha transcriptional target, modulates T-box factor activity in orofacial clefting. PLoS Genet *9*, e1003785.

Wang, J., Greene, S.B., Bonilla-Claudio, M., Tao, Y., Zhang, J., Bai, Y., Huang, Z., Black, B.L., Wang, F., and Martin, J.F. (2010). Bmp Signaling Regulates Myocardial Differentiation from Cardiac Progenitors Through a MicroRNA-Mediated Mechanism. Developmental Cell *19*, 903-912.

Williams, J.M., de Leeuw, M., Black, M.D., Freedom, R.M., Williams, W.G., and McCrindle, B.W. (1999). Factors associated with outcomes of persistent truncus arteriosus. Journal of the American College of Cardiology *34*, 545-553.

Xiao, C., Srinivasan, L., Calado, D.P., Patterson, H.C., Zhang, B., Wang, J., Henderson, J.M., Kutok, J.L., and Rajewsky, K. (2008). Lymphoproliferative disease and autoimmunity in mice with increased miR-17-92 expression in lymphocytes. Nat Immunol *9*, 405-414.

Yamagishi, H., Maeda, J., Uchida, K., Tsuchihashi, T., Nakazawa, M., Aramaki, M., Kodo, K., and Yamagishi, C. (2009). Molecular embryology for an understanding of congenital heart diseases. Anatomical Science International *84*, 88-94.

Yanagisawa, H., and Davis, E.C. (2010). Unraveling the mechanism of elastic fiber assembly: The roles of short fibulins. The International Journal of Biochemistry & Cell Biology *42*, 1084-1093.

Zhang, H., and Bradley, A. (1996). Mice deficient for BMP2 are nonviable and have defects in amnion/chorion and cardiac development. Development *122*, 2977-2986.

Zhao, Y., and Srivastava, D. (2007). A developmental view of microRNA function. Trends Biochem Sci *32*, 189-197.

Zhou, j., Pashmforoush, M., and Sucov, H.M. (2012). Endothelial neuropilin disruption in mice causes DiGeorge syndrome-like malformations via mechanisms distinct to those caused by loss of Tbx1. PLoS ONE *2012;7(3):e32429*.

Zwijsen, A., Verschueren, K., and Huylebroeck, D. (2003). New intracellular components of bone morphogenetic protein/Smad signaling cascades. FEBS Letters *546,* 133-139.

APPENDIX

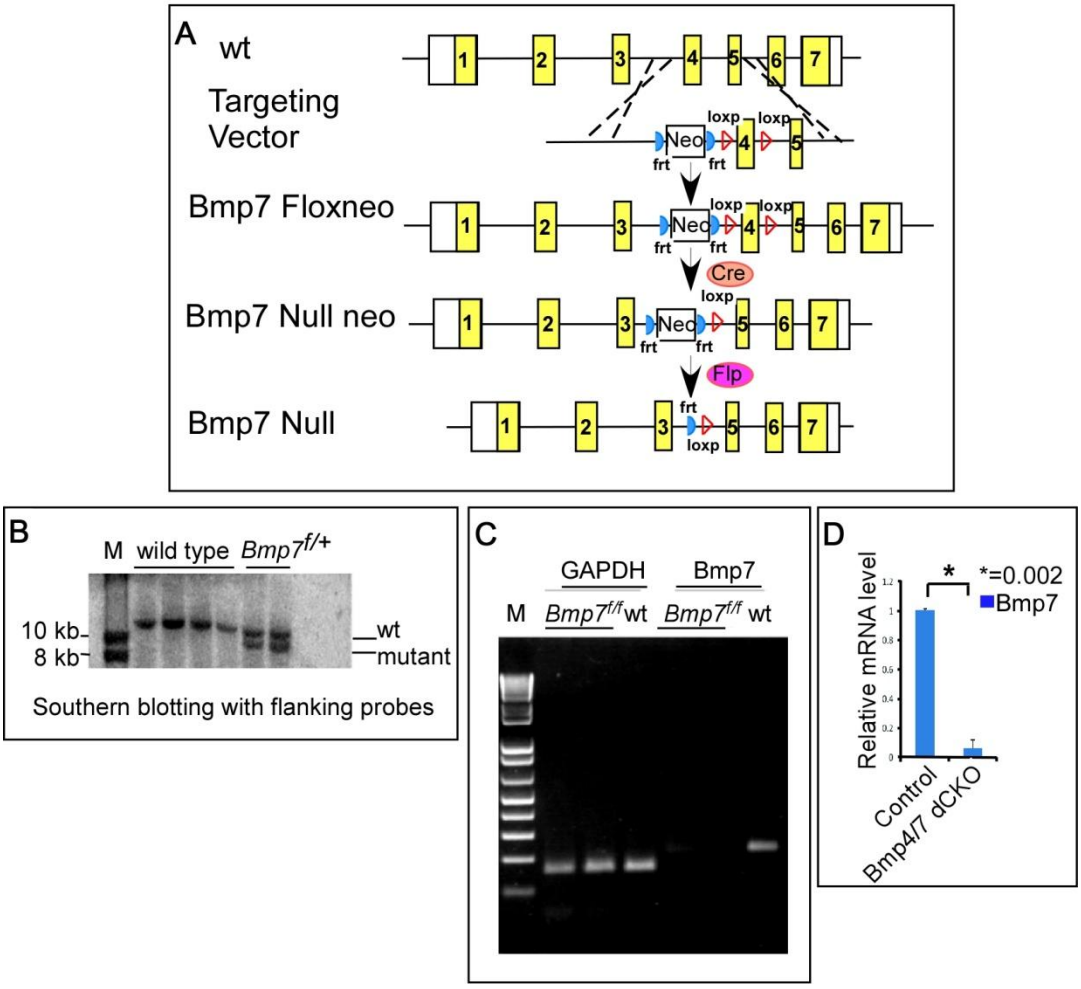

A-1: Targeting scheme for the inactivation of *Bmp7*. A: Targeting Strategy for *Bmp7* ablation. **B**: Southern blot analysis of Bmp7flox allele. **C**: qRT-PCR analysis of Bmp7 in wild type and knockout samples. **D**: quantification of Bmp7 mRNA level.

A-2: Oligos used for gene amplification, ChIP-PCR and qRT-PCR

Primer	Sense (5'-3')	Antisense (5'-3')
VEGFA-promoter	AGGGTACCAGGGGACAGAGCCACA	ACCTCGAGCACGATTTAAGAGGGG
VEGFA-3'UTR	GTACTAGTGCCAGGCTGCAGGAAGGAGCCTCCCTCAGGGTTT	GGACGCGTTTTGAGATCAGAATTCAATTCTTTAATACAAA
s1-mut	CTGGCCTACCTACCTTTCTGAGGTTTAGGGTAGGTTTGAATCACC	GGTGATTCAAACCTACCCTAAACCTCAGAAAGGTAGGTAGGCCAG
SBE1-mut	CAGGAGGAACAAGGGCCTCTGAATTCCCAGCTGTCTCTCCTTCAG	GAAGGAGAGACAGCTGGGAATTCAGAGGCCCTTGTTCCTC
SBE2-mut	CTCCTTCAGGGCTCTGCCTCGAGACACAGTGCATACGTGG	CCACGTATGCACTGTGTCTCGAGGCAGAGCCCTGAAGGAG
SBE3-mut	CGTGAACTTGGGCGAGCCGAAATTTCGTGAGGGAGGACGCGTGTG	CACACGCGTCCTCCCTCACGAAATTTCGGCTCGCCCAAGTTCACG
3'UTR-mut	GGAGACTCTTCGAGGACTCGAGCGGGTCCGGAGGGCGAGACTCCGG	GGAGACTCTTCGAGGACTCGAGCGGGTCCGGAGGGCGAGACTCCGG
Site1-ChIP	TGGGAGGACAGAGTACACCCCTGA	CAGAGGCCCTTGTTCCTCCTGA
Site2-ChIP	GGCACCCTGGCTTCAGTTCCC	TGCGTGTTTGACCTCGGAAGC
Site3-ChIP	CCCCTTTCCAAGACCCGTGCC	ACCCCTGGCTTTCTCCCCCA
Id1	CCGCTCAGCACCCTGAACGG	CCCCTGGGGAACCGAGAGCA
Id2	TCCAGGACGCCGCTGACCA	CAACGTGTTCTCCTGGTGAAATGGC
Slug	GCACTGTGATGCCCAGTCTA	CAGTGAGGGCAAGAGAAAGG
Snai1	AAACCCACTCGGATGTGAAG	GAAGGAGTCCTGGCAGTGAG

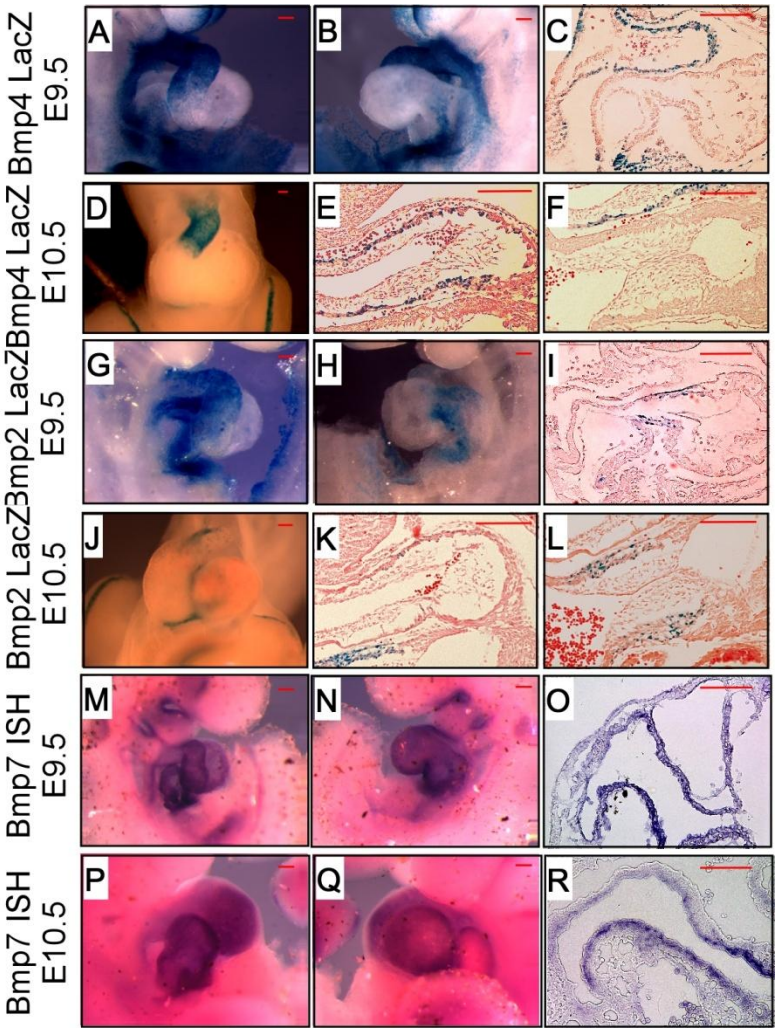

A-3: Expression of *Bmp2/4/7* in the heart at E9.5 and E10.5. (A-F): *Bmp4* is expressed in second heart field (SHF), out-flow tract (OFT), in-flow tract (IFT) and right ventricle (rv) at E9.5. Sections reveal that *Bmp4* is exclusively expressed in myocadium but not in endocardium or cushion mesenchyme of the OFT. (G-L): *Bmp2* is expressed in the OFT and AV cushion in both E9.5 and E10.5 embryos. Its expression in the OFT is limited. (M-R): In situ hybridization of *Bmp7* probe shows that *Bmp7* is broadly expressed in the entire heart tube. At E10.5, *Bmp4* expression is restricted to the myocardium of OFT; *Bmp7* expression is similar to its E9.5. Scale bar=100 μm.

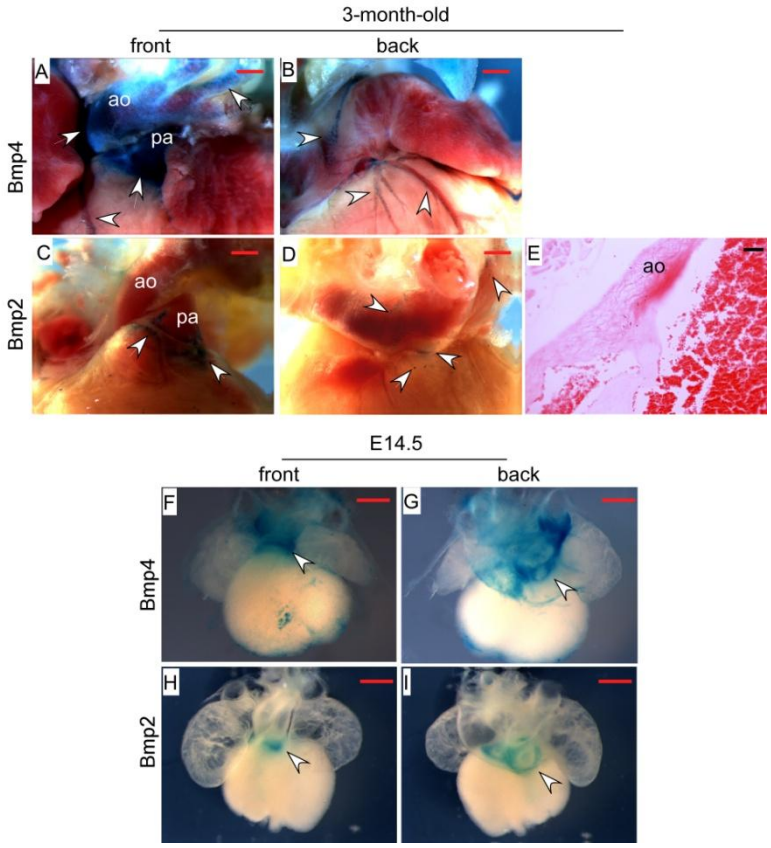

A-4: Bmp4 is expressed in pulmonary and aorta during development. (**A**-**E**): Bmp4 and Bmp2 expression pattern at E14.5. Hearts from $Bmp4^{LacZneo/+}$ and $Bmp2^{LacZneo/+}$ embryos are harvest at E14.5 and performed LacZ staining. Whole mount images are taken afterwards. Scale bar (red)=500μm. (**F**-**I**): Hearts from $Bmp4^{LacZneo/+}$ and $Bmp2^{LacZneo/+}$ adult mice are dissected at 3 month old. Hearts are then embedded and sectioned (G and J). Blue is lacZ positive. Scale bar (red)=500 μm, scale bar (black)=50μm. ao: aorta; pa: pulmonary.

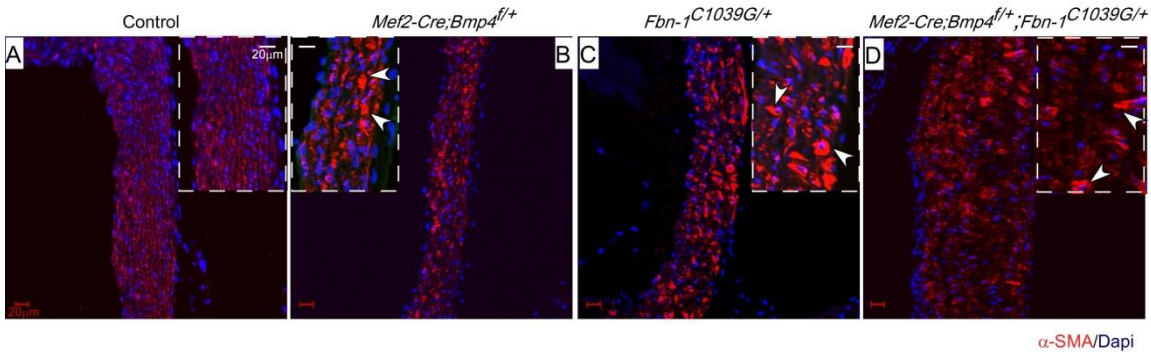

A-5: Abnormal Assembly of SMCs in Bmp and Fbn mutants. (A-D): boxed area is higher magnification. Scale bar =20 μm.

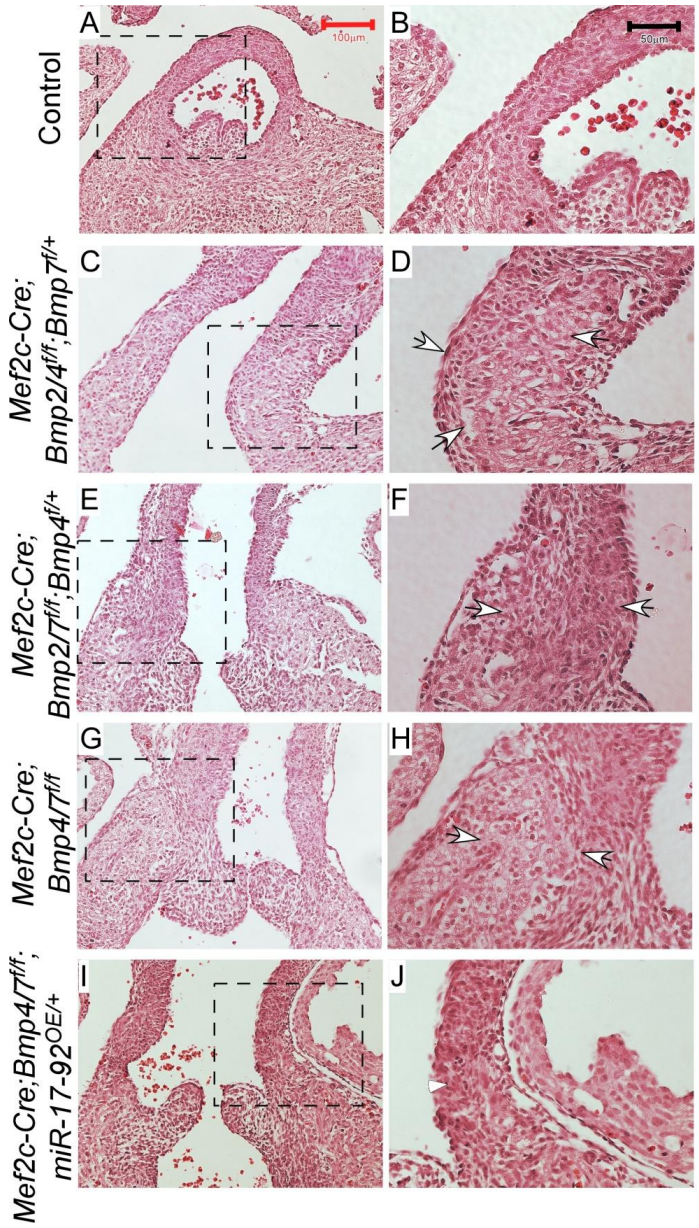

A-6: Bmp deficiency results in abnormal truncus morphology. (**A**-**J**): morphology of different compound mutants of Bmp. panel B, D, F, H, J are zoomed-in images of panel A, C, E, G, I, respectively. Arrows in D, F, H show abnormal morphology of trunks vessel wall in Bmp mutants. Arrowheads in J show mild phenotype comparing to D, F, and H. Scale bar (white)= 100 μm; Scale bar (red)=50 μm.

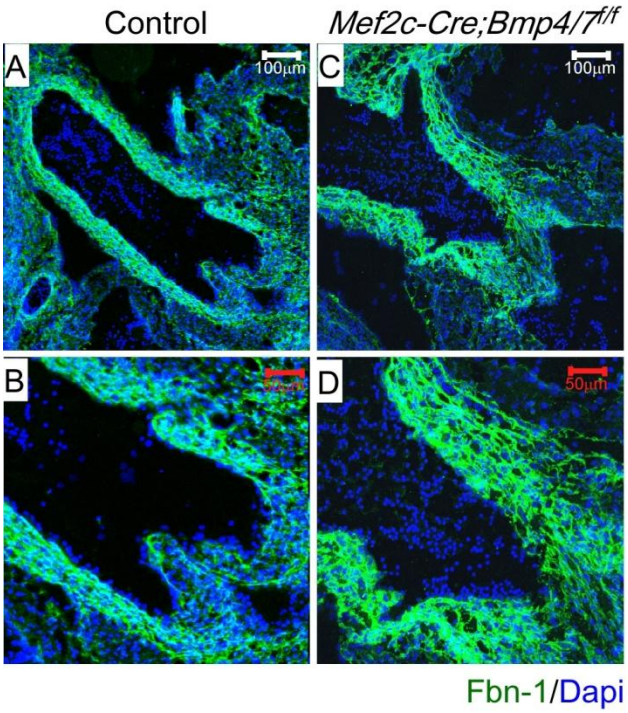

A-7: Fbn-1 expression is not affected in the absence of Bmp4/7. (A-D): Immunostaining of Fbn-1 on Bmp4/7 dCKO at E14.5. Scale bar (white) =100 μm; Scale bar (red) = 50 μm.

A-8: Putative Smad binding sites in Fbn upstream sequence. Smad binding elements sequence CAGAC/GTCTG are conserved among several species. Smad1 binding site sequence is ATGC, and GC rich box is GCCG.

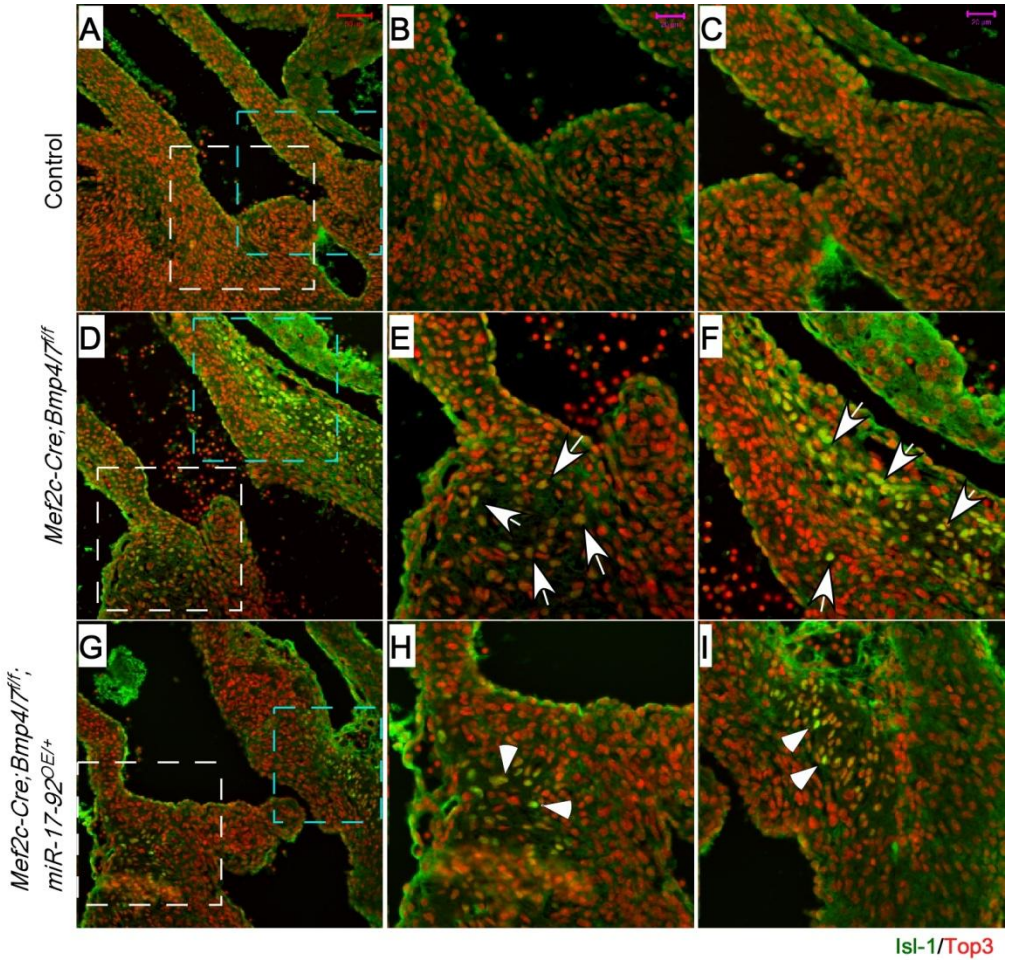

A-9: miR-17-92 overexpression represses Isl-1. Arrow heads point to Isl-1 positive cells. Middle panel is zoomed-in images of white boxed area, right panel is zoomed-in images of blue boxed area. Scale bar (red)=100 μm; purple=50 μm.